Chem

Size-selective Catalytic Polymer Acylation with a Molecular Tetrahedron

Mona Sharafi,[1] Kyle T. McKay,[1] Monika Ivancic,[1] Dillon R. McCarthy,[1] Natavan Dudkina,[1] Kyle E. Murphy,[1] Sinu C. Rajappan,[1] Joseph P. Campbell,[1] Yuxiang Shen,[2] Appala Raju Badireddy,[2] Jianing Li,[1,*] and Severin T. Schneebeli[1,3,**]

[1]Department of Chemistry, University of Vermont, Burlington, VT 05405, USA
[2]Department of Civil and Environmental Engineering, University of Vermont, Burlington, VT 05405
[3]Lead Contact
*Correspondence: jianing.li@uvm.edu
**Correspondence: severin.schneebeli@uvm.edu

SUMMARY

Selective catalysis at the molecular level represents a cornerstone of chemical synthesis. However, it still remains an open question how to elevate tunable catalysis to larger length scales to functionalize whole polymer chains in a selective manner. We now report a hydrazone-linked tetrahedron with wide openings, which acts as a catalyst to size-selectively functionalize polydisperse polymer mixtures. Our experimental and computational evidence supports a dual role of the hydrazone-linked tetrahedron. To accelerate functionalization of the polymer substrates, the tetrahedron (i) unfolds the polymer substrates and/or breaks the polymer aggregates as well as (ii) enables target sites (amino groups) on the polymers to coordinate with catalytic units (triglyme) attached to the tetrahedron. With the tetrahedron as the catalyst, we find that the reactivity of the shorter polymers increases selectively. Our findings enable the possibility to engineer hydrolytically stable molecular polyhedra as organocatalysts for size-selective polymer modification.

Keywords: Substrate-selective catalysis; Polymeric substrates; Post synthetic polymer modification (PSPM); Hydrazone-linked molecular cage; Glyme catalysis; molecular dynamics simulations; Supramolecular chemistry

INTRODUCTION

Selective catalytic chemical modification after synthesis represents[1-2] an effective means to diversify the structures and functions of small molecules and polymers. Yet, despite various examples of protein posttranslational modifications (PTMs) catalyzed by enzymes, it remains a daunting task to create catalysts that can selectively recognize and modify man-made polymers. Thus, it has been a major goal of synthetic chemists to create supramolecular catalysts,[3-7] which can operate selectively on man-made polymers.[8-9] These efforts have led to the successful application of selective supramolecular catalysts for small-molecule transformations[10-18] as well as for growth[8, 19-20] and functionalization[9, 21] of linear polymers in a processive manner. However, selective post-synthetic polymer modification (hereafter referred to as PSPM) by supramolecular organocatalysts has, to the best of our knowledge, not yet been reported. We now show that a hydrazone-linked tetrahedron with large openings can size-selectively functionalize (Figure 1b) complex polymeric mixtures. Analogous to previously-reported catalytic transport systems operating with polymeric tracks[21-22] our

catalyst is designed to slide along the polymeric substrates during the reaction, which leads to efficient (Figure 6) catalytic functionalization of side-chain functional groups.

This process is enabled — like in the seminal system of Nolte and coworkers[19-21]— by threading of the polymer chains through the cavity of the catalyst. Yet, in contrast to Nolte's catalyst, which was optimized for linear polymers, threading and size-selective functionalization of side-chains polymers also becomes possible with our organocatalytic tetrahedron. In regards to prior work in the field of size-selective catalysis (which has recently been reviewed[17] by Otte) our system is unique in that it acts on a polydisperse mixture of polymer chains in a size-selective manner, while mostly pairs of small-molecules were used as the substrates for size-selective catalysis in prior work (see the examples shown in Figure 1a).

To achieve activity and selectivity, a PSPM catalyst has to recognize the polymeric substrates to initiate catalysis. Molecular polyhedra with large opening are well suited to meet this challenge with tetrahedral structures providing the largest openings out of all possible regular polyhedra.[4] For instance, the surface area per face of a tetrahedron is 1.8 times larger than the corresponding surface area per face for a cube with an identical volume. Here we now show that — due to their wide openings — tetrahedral cages allow polymers with bulky side chains to thread through, to prepare for further catalytic functionalization. Although molecular polyhedra with T_d symmetry can be synthesized[23-28] with dynamic covalent chemistry (e.g. with imine linkages)[23, 29-38], the currently reported systems lack sufficient stability[39-40] for organocatalytic PSPM processes.[41] While hydrolytic stability can be imparted onto imine-linked cages by reduction of the imines to amines,[37-38, 42] the secondary amines formed upon reduction are good nucleophiles, which would engage in side-reactions under the acylation conditions employed in this work. Thus, rather than using cages with imine/amine linkages, we first invented a method to create a porous tetrahedron (Figure 2) with acyl-hydrazone linkages and peripheral glycol chains required for the PSPM catalysis. The primary reasons for utilizing a hydrazone-linked cage[43-46] as our organocatalyst were the following: (i) Hydrazone linkages generally display enhanced hydrolytic stability, which renders them excellent candidates for catalysis. (ii) The NH group available in acyl-hydrazones represents a suitable hydrogen bond donor, which can direct the assembly of hydrazone-linked polyhedra. (iii) The hydrogen bonding capabilities of hydrazones can assist PSPM catalysis by binding and unfolding polymeric substrates.

However, due to the hydrogen bonding capabilities of hydrazones, hydrazone-linked cages with large openings[47] (see Figure 2 for models minimized with the OPLS3[48] force field) have a high propensity to form interlocked structures.[49-50] This feature renders it difficult to synthesize hydrazone-linked cages without intercatenation, which is one reason for why hydrazone-linked polyhedra with large openings and T_d symmetry are challenging to synthesize. The closest design to a tetrahedral hydrazone-linked cage is (see Figure 2a) the C_{2d} symmetrical hydrazone cavitand **Cage-1**, invented[47] by Warmuth and coworkers. Yet, with ca. 9–13 Å (Figure 2a) the openings of **Cage-1** are relatively narrow, which prevents intercatenation but would likely also prevent side-chain polymers from threading through as required for PSPM catalysis.

For an efficient synthesis of hydrazone-tetrahedra (Figure 2b) with large openings, we designed a special vertex (*syn*-**7)** to encode tetrahedron formation (Scheme 1). *Syn*-**7** combines hindered rotation[51] around three Ph-Ph σ-bonds with three intramolecular [NH...OR]-hydrogen bonds, which direct[44] the growth of the tetrahedron upon hydrazone formation. This strategy allowed us to create a

hydrazone-linked T_d-symmetric molecular tetrahedron. The tetrahedron not only binds to side-chain polymers but it also catalyzes the PSPM of amine-functionalized polymers with relatively long side-chains in a size-selective manner.

RESULTS

Synthesis of a Hydrazone-linked Molecular Tetrahedron

The synthesis (Scheme 1, see Figures S30–S61 for spectroscopic characterization data) of *syn*-**7** started with a trifold formylation of *syn*-**1**, which is created on a large scale with a solid state-driven amplification of the *syn*-atropoisomer of **1** as we reported[51] previously. The methoxyl groups *ortho* to the aldehydes of the resulting *syn*-**2** were then removed selectively with BCl_3 to afford the tris-phenol *syn*-**3**. Finally, *syn*-**3** was converted into the vertex *syn*-**7** through (i) alkylation of the phenolic -OH groups, (ii) Pinnick oxidation[52] of the aldehydes to carboxylic acids, (iii) esterification, and (iv) hydrazinolysis of the resulting methyl esters. To form the tetrahedron **Tet-1**, we mixed two equivalents of the vertex *syn*-**7** with three equivalents of terephtalaldehyde and trifluoroacetic acid (TFA) as the catalyst in CH_2Cl_2. After 48 h of stirring at room temperature, **Tet-1** formed in 80% yield, as confirmed (see the Supplemental Experimental Procedures section as well as Figures S2, S44, and S45) by high-resolution (HR) electrospray ionization (ESI) mass spectrometry (MS) as well as ^{1}H, ^{13}C and diffusion-ordered spectroscopy (DOSY) nuclear magnetic resonance (NMR) spectroscopy.

The ^{1}H-NMR spectrum of **Tet-1** (Figure S44) illustrates its T_d symmetry with only five resonances (all singlets) appearing in the region between 6 and 12 ppm. Based on a minimized molecular model (Figure 2b), the height of **Tet-1** is 22 Å which agrees well with the solvodynamic diameter (21 Å) measured by DOSY ^{1}H-NMR spectroscopy (Figure S2). The cage is not only soluble in organic solvents but also in aqueous mixtures with polar organic solvents. To test its hydrolytic stability, we therefore dissolved **Tet-1** in a 90:10 vol-% mixture of DMSO-d6 and D_2O and heated the resulting clear solution to 80 °C for 5 h. No degradation was observed (Figure S1) under these conditions by ^{1}H-NMR spectroscopy, which illustrates the excellent hydrolytic stability of **Tet-1**, even at elevated temperatures.

Polymer Recognition with Tet-1

With **Tet-1** isolated, we embarked on investigating the molecular tetrahedron's ability to recognize amine-functionalized polymers with side chains, since binding to such macromolecules is a prerequisite for the catalytic polymer functionalization described below. To create amine-functionalized polymers, we first condensed 1-aminooctane (90 mol %) with commercial poly(isobutylene-*alt*-maleic) anhydride, and then reacted (Scheme 2) the remaining anhydride units with 1,6-diaminohexane. As shown by (i) elemental analysis, (ii) by IR spectroscopy, and (iii) by measuring the percentage of free amino groups through complete acylation at elevated temperature, this procedure (detailed in the experimental procedures section) leads to full and partial amidation of the maleic anhydride units to afford a polydisperse mixture of amine-functionalized poly(isobutylene-*alt*-*n*-octyl maleamide) (**NH_2-POA**) polymers with an $\overline{M}_w$ (DOSY-^{1}H-NMR)[53] of 6.3 kDa. The polymeric mixture is well-soluble in a variety of organic solvents and contains 3.7 repeat units (out of 20.5) with free NH_2-containing sidechains on average.

Next, binding between **Tet-1** and the polymeric **NH_2-POA** substrate was confirmed with (i) DOSY ^{1}H-NMR spectroscopy (Figures 3a–c), (ii) ^{1}H-^{1}H-NOESY NMR spectroscopy (Figure 3d), (iii) all-atom molecular dynamics (MD) simulations (Figure 4), as well as (iv) ^{1}H-NMR-based host-guest titrations (Figure 5). The DOSY ^{1}H-NMR

spectrum of the **NH_2-POA/Tet-1** mixture shows two diffusion bands for the [**NH_2-POA@Tet-1**] complex at different diffusion coefficient (D) values (1.7 x 10^{-10} m^2 s^{-1} and 2.5 x 10^{-10} m^2 s^{-1}). These two diffusion bands of the complex arise from two different complexation geometries, which interconvert slowly on the NMR timescale. Based on a direct comparison with MD simulations (*vide infra*), the larger complex, with an average D value of 1.7 x 10^{-10} m^2 s^{-1}, is the one where **NH_2-POA** is threaded through the cavity of **Tet-1**. For this binding geometry, we clearly observed (see: Figure 3d and Figure S7) NOE cross peaks between the H_c protons of **Tet-1** (which point straight into the cavity of the molecular tetrahedron) and the aliphatic protons ($H_{Poly\text{-}aliphatic}$) of the polymer chains. This finding supports threading of the polymer chains through the cavity of **Tet-1**. In general, the NOE cross-peaks between the protons of the polymers and **Tet-1** (especially with H_d) are stronger (*cf.* Figures 3d and S7) with the shorter polymers (**Short-NH_2-POA**). Thus, since the longer polymers bind the strongest (Figure 5b) to **Tet-1**, they very likely interact (see Figure 4d for a simulated structure of the complex with a long polymer chain) not only with the inside, but also with the outside of cage. In turn, the shorter polymers are not long enough to effectively wrap around the tetrahedron, while at the same time threading through **Tet-1**'s cavity, which leads (*vide infra*) to a more active catalytic conformation with the shorter polymer chains.

In the threaded binding geometry, the solvodynamic diameter of **NH_2-POA** increases by ca. 50%, compared to the solvodynamic diameter of the **NH_2-POA** polymer on its own (Figure 3c). To confirm this finding, we ran MD simulations (Figure 4) of the polymer with and without **Tet-1** for 800 ns. These simulations demonstrated that the observed increase in polymer size[50] (ca. 20% size-increase is predicted by the MD simulations) is indeed caused by unfolding of the polymer, when it threads through **Tet-1**. As also indicated by the MD simulations, the polymer-unfolding is driven (Figure S29) by the cage breaking up the intramolecular hydrogen bonds in the polymer, and replacing them with polymer-to-cage hydrogen bonds. Further support for this finding is provided by (i) Figure S10, which shows that when DMSO-*d6* (a well-known hydrogen-bond disruptor) is added to a solution of the [**NH_2-POA@Tet-1**] complex in CD_2Cl_2, rapid decomplexation occurs as well as (ii) by Figure S28, which demonstrates that **Tet-1** no longer serves as an effective catalyst in a polar solvent like DMSO-d6. In the second diffusion band, the diffusion coefficient (D) of the polymer decreases only slightly, compared to the D of the polymer by itself, from 2.8 x 10^{-10} m^2 s^{-1} (unbound polymer, Figure 3c) to 2.5 x 10^{-10} m^2 s^{-1} (bound polymer, Figure 3b). Thus, we conclude that in the second binding conformation, the polymer gets unfolded to a lesser extent then when it is threaded through the cage, likely because the polymer and **Tet-1** interact with side-on coordination modes in the second binding conformation.

To gain further insight into the nature of the polymer recognition abilities of **Tet-1**, we separated and isolated (as detailed in the experimental procedures section) the shortest (**Short-NH_2-POA**, $\overline{M}_w$ = 2.6 kDa) and longest (**Long-NH_2-POA**, $\overline{M}_w$ = 9.9 kDa) fractions contained in the original **NH_2-POA** sample with an additional size-exclusion chromatography run. We then titrated both the short and long polymer samples into 0.28 mM solutions of **Tet-1** in CD_2Cl_2 while recording the ^{1}H-NMR spectra of the mixtures at each titration point. The titration curves obtained (see Figures 5a) show that the polymer resonances shift downfield[54] when the polymer threads through the cavity of **Tet-1**. This finding is explained (Figure 5c) by the detailed structure and associated aromatic ring-current effects[55] of the threaded binding geometry, wherein the polymer chain passes by the side (and not the face as in most small-molecule pseudo-rotaxanes/rotaxanes[56-57]) of the aromatic linkers in **Tet-1**.

Analysis of the NMR titration data (Figure 5b) with the LineshapeKin 4.0[58] software (fit to a simple 1:1 binding model) in combination with the curve-fit algorithm

implemented in the SciPy 0.18 package[59] provided further information regarding the complexation thermodynamics and kinetics between the **NH₂-POA** polymer substrates of different lengths and the **Tet-1** catalyst. First, we discovered that the shorter polymer chains ($\overline{M}_w$ = 2.6 kDa) de-complex nearly three times as fast as the longer ($\overline{M}_w$ = 9.9 kDa) ones (see Figure 5b for the de-complexation rate-constants, k_{off}, measured for **Short-** and **Long-NH₂-POA**). This result represents further evidence for pseudorotaxane formation between **Tet-1** and the **NH₂-POA** polymers, as de-threading from a pseudorotaxane-like conformation is expected[60] to slow down with increasing polymer length, since it takes longer on average for **Tet-1** to slide to the end of a longer polymer chain. Second, the complex association constants (K_a) determined (Figure 5) by the ^{1}H-NMR titration experiments demonstrated that the longer **NH₂-POA** polymer chains bind stronger to **Tet-1** than the shorter ones. Interestingly, for enzymes, it is well-known[61] that if an enzyme binds too strongly (i.e. too "tight") to its substrate (but not as strongly to the transition state), the enzymatic reaction will slow-down with increasing substrate-binding strength. Here, we now observe a similar phenomenon (Figure 9d) for a fully synthetic system. Specifically, we discovered (*vide infra*) that the shorter **NH₂-POA** polymers (which bind the weakest to the **Tet-1** catalyst) nevertheless react the fastest with **Tet-1**. Overall, this section provided evidence that **Tet-1** is able to thread-over and partially unfold/stretch out the **NH₂-POA** polymers in CD_2Cl_2 (which is an ideal solvent for glyme-catalyzed aminolysis), laying the foundation to use **Tet-1** as a size-selective organocatalyst as described below.

Organocatalytic Polymer Functionalization with Tet-1

Triglyme functional groups act[62] as organocatalysts to accelerate aminolysis reactions. Since **Tet-1** possesses 12 peripheral triglyme chains and binds to amine-functionalized **NH₂-POA** polymers, **Tet-1** can engage in size-selective catalytic (Figure 6) functionalization of these polymeric substrates. We evaluated the catalytic performance of **Tet-1** by monitoring the kinetics of the aminolysis reaction with ^{1}H-NMR in the presence of an internal standard (1,2,4,5-tetrabromobenzene, TBB). Five reaction mixtures were prepared in CD_2Cl_2 as the solvent. Each of the reaction mixtures contained (i) an excess of 4-nitrophenyl-3,5-dinitrobenzoate (NDB) active ester, (ii) **NH₂-POA** polymer as the substrate, as well as (iii) one of the following catalysts/controls: a) **Tet-1**, b) **Edge-Model** (a model for an edge of **Tet-1**), c) **Triglyme** + a simple control hydrazone (**Control**) in equimolar amounts, d) **Triglyme** by itself, and d) no additives. We selected NDB as the active ester, since it attaches dinitrobenzoate groups onto the polymers, which are readily observed in the aromatic region of the spectrum in DOSY ^{1}H-NMR. This fact enabled us to determine (*vide infra*) the size-selectivity of the polymer-functionalization reactions.

We followed the progress of the reactions by integrating (see Figures S13–S26) the distinct ^{1}H-NMR resonance at 6.9 ppm, which corresponds to *p*-nitrophenol formed upon aminolysis of the NDB active ester. From the *p*-nitrophenol concentration and the initial amine concentration ($[amine]_0$ = 1.8 mM), the concentrations of the remaining amino groups ([amine]) on the **NH₂-POA** polymers were calculated for each time point. Our kinetic data shows that plots of $[amine]^{-1}$ *vs.* reaction time (Figure 6a) are linear for all the samples and therefore the reactions are all second order in the amine-concentration. The amino groups on the polymers are therefore not just acting as the reagent for aminolysis, but also as catalysts to deprotonate[62] the tetrahedral amine-adducts. Furthermore, we found by changing the catalyst concentrations (see Figures S27B and C for the corresponding rate-plots) that the reactions are approximately first order in the catalyst concentration for the simple

Triglyme + **Control** as well as for the **Edge-Model** catalysts. This result is in line with the prior literature for glyme-catalyzed aminolysis reactions.[62] However, with **Tet-1** as the catalyst, we discovered (Figure S27A), that the reaction is not just second order in the amine concentration, but also second order in the **Tet-1** concentration. Given this information, we can[63-64] write the rate-laws for the PSPM reactions with cat = **Edge-Model** or **Triglyme** as:

$$\frac{\partial[\text{amine}]}{\partial t} = k_{\text{obs}}[\text{cat}]_0[\text{amine}]^2 \quad \text{(Eq. 1)}$$

On the other hand, with cat = **Tet-1**, the rate law can be written as:

$$\frac{\partial[\text{amine}]}{\partial t} = k_{\text{obs}}[\text{cat}]_0^2[\text{amine}]^2 \quad \text{(Eq. 2)}$$

Finally, for the control reaction without any catalyst added, we define the rate constant k_{obs} of the reaction in an analogous manner:

$$\frac{\partial[\text{amine}]}{\partial t} = k_{obs}[\text{amine}]^2 \quad \text{(Eq. 3)}$$

k_{obs} in equations 1–3 are observed rate constant (defined in equation S3), [amine] is the total concentration of amino groups on all the polymer chains, and $[cat]_0$ is the initial concentration of the organocatalyst. The rate constants k_{obs} (Table 1) and slopes obtained from the second-order rate-plots (Figure 6a) demonstrate that acylation of the amines on the polymers with **Tet-1** as the catalyst is significantly faster than with any of the other control reactions. Thus, **Tet-1** is a more effective catalyst than either simple **Triglyme** or the **Edge-Model**, both of which lack the large cavity of the hydrazone cage.

Size-selectivity of the Organocatalytic Polymer Functionalization Process

We have been able to demonstrate that the **Tet-1** catalyst can distinguish between different chain-lengths of the **NH_2-POA** substrates directly in the complex mixture of all the polymer chains and partially reverse the intrinsic size selectivity for the catalytic polymer functionalization process. Our evidence for the size selectivity includes:

(i) A distinct difference (Figure 7) in the average solvodynamic diameter for the polymers functionalized with **Tet-1**, compared to the polymers functionalized with the control catalysts.

(ii) DOSY ^{1}H-NMR spectra (Figure 8), which confirm directly that — *when the reaction is executed with the real polymer mixture* — the functionalized polymers display a smaller solvodynamic diameter than the unfunctionalized ones when **Tet-1** is used as the catalyst.

(iii) Explicit measurements (Figure 9) of all the catalytic rate constants, k_{obs}, for the short and long polymer chains with all catalysts (**Tet-1**, **Edge-Model**, and **Triglyme**).

(i) Evidence of Size-selectivity Based on Solvodynamic Diameters

To investigate the size selectivity in the presence of all polymer chains, we first ran PSPM reactions with different catalysts and NDB as the acylation reagent to the exact same conversion (24%). For the first catalytic system, **Tet-1** (0.28 mM) was used as the catalyst, while a combination of **Triglyme** + **Control** (3.4 mM each) was used as

the control. To be able to directly compare the different reaction systems, we equalized them before analysis with the following protocol: (i) For the functionalization reaction catalyzed by **Tet-1** (0.28 mM), we added **Triglyme** (3.4 mM) and **Control** (3.4 mM) just before analysis. (ii) For the control reaction catalyzed by **Triglyme** (3.4 mM equivalents) + **Control** (3.4 mM), we added **Tet-1** (0.28 mM), again just before analysis. All measurements were executed with volumetric additions from identical stock solutions. In this manner we ensured that, besides the differently-functionalized polymers, all other components and amounts thereof were exactly the same for all the samples in the end. As a result, different properties of the equalized reaction mixtures are expected to directly correlate with differences in the functionalization patterns of the polydisperse **NH_2-POA** substrates.

DOSY ^{1}H-NMR spectra of all reaction mixtures were recorded immediately after equalization. From these spectra, the average solvodynamic diameters of the polymers were determined. Significant differences in the solvodynamic diameters of the polymers were observed between the control reaction and the **Tet-1**-catalyzed variant. *These differences indicate (Figure 7) a change in size-selectivity for polymer functionalization with **Tet-1**:* With the control reaction, the longer polymer chains get acylated the fastest, which results in a significant reduction of the number-averaged solvodynamic diameter of the polymer (from 4.9 to 2.8 nm) upon acylation of the amines. This reduction in polymer size can be explained with less aggregation occurring after acylation (since fewer strong [-NH_2…HOOC-]-hydrogen bonds are present after acylation) and the fact that longer polymers have a higher tendency to aggregate, because they contain more NH_2 and COOH groups on average than shorter ones. A much smaller reduction in the solvodynamic polymer diameter upon acylation (from 4.9 to 4.5 nm) is observed for functionalization with **Tet-1** as the catalyst. This finding indicates that, with **Tet-1** as the catalyst, shorter polymer chains (which have a weaker tendency to aggregate) get acylated the fastest.

(ii) Comparing the Diffusion Constants of the Functionalized to the Unfunctionalized Polymers Provides Direct Evidence for Size Selectivity in the Polydisperse Mixture

To obtain additional evidence for the size-selectivity in the polymer mixture, we compared (Figure 8) the average size of the functionalized polymer chains to the average size of all the polymer chains (both functionalized and unfunctionalized) with DOSY ^{1}H-NMR spectroscopy. We acylated with NDB — which attaches 3,5-dinitrobenzamide units with distinct aromatic ^{1}H-NMR resonances to the polymers. Thus, we were able to determine the average diffusion constant of the functionalized polymers from the DOSY ^{1}H-NMR resonances of the 3,5-dinitrobenzamide units. The results obtained clearly show (Figure 8) that the aromatic resonance corresponding to the *acylated* **NH_2-POA** substrates is lined up with the shorter polymer chains of the sample when **Tet-1** is used as the catalyst. In contrast, when **Triglyme** + **Control** are used as the catalysts instead, the medium/longer polymer chains react faster in the PSPM reaction.

*(iii) Measurements of the Relative Rate Constants for the Acylation of Short and Long Polymers Separately Confirm **Tet-1**'s Selectivity for Shorter Polymers*

We had managed to isolate (see Figure 5 as well as the experimental procedures section) some of the shortest (**Short-NH_2-POA**; $\overline{M}_w$ = 2.6 kDa) and longest (**Long-NH_2-POA**; $\overline{M}_w$ = 9.9 kDa) polymer chains contained within the original **NH_2-POA** sample. Thus, we were able to measure (Figure 9) the acylation rate constants of the short and long polymer samples separately, analogous to how we determined (Figure 6) the rate constants (k_{obs}) with the mixed **NH_2-POA** sample.

The results shown in Figure 9 tell us the following:

(i) The short polymers (**Short-NH_2-POA**; k_{obs} = 2.9 ± 0.4 x 10^9 M^{-3} h^{-1}) indeed react faster with the **Tet-1** catalyst than the longer ones (**Long-NH_2-POA**; k_{obs} = 1.9 ± 0.3 x 10^9 M^{-3} h^{-1}), which confirms the size-selectivity determined directly (see Figures 7 and 8) in the polymer mixture.

(ii) We see that the longer chains intrinsically react faster than the shorter ones, if we take the reactivity with the small **Triglyme** catalyst as a measure for the intrinsic reactivity of the polymer chains. This finding once again agrees with the conclusions from the DOSY ^{1}H-NMR measurements (Figures 7 and 8). We hypothesize that the longer polymer chains intrinsically react faster than the shorter ones, since they contain more amino-groups per polymer chain on average, which are needed (Scheme 3) for intramolecular base-catalysis.

(iii) Overall, the rate constants determined for the short and long polymer chains by themselves are faster with all the catalysts than with the mixed polymer sample. This finding tells us that the mixture does not behave exactly like its individual components, which is expected for a complex system with many interacting parts. For example, we know that the longer polymer chains bind (Figure 5b) stronger to the **Tet-1** catalyst than the shorter ones. Nevertheless, the shorter chains react faster with the catalyst, as weaker binding to the substrate helps to further lower[61] (Figure 9d) the activation Gibbs free energy of the reaction. Thus, from the measured binding and rate constants, we can conclude that the longer polymers must inhibit the reaction with the shorter polymers, which is likely why the rate constant for the shorter polymers alone with **Tet-1** (k_{obs} = 2.9 ± 0.4 x 10^9 M^{-3} h^{-1}) is indeed larger than the rate constant of the mixture (k_{obs} = 8.3 ± 0.8 x 10^8 M^{-3} h^{-1}) with **Tet-1**.

(iv) The relative rate-plot-slopes obtained with the three different catalysts also provide (see Figures 3 and 4 for additional evidence) direct evidence for polymer unfolding by **Tet-1** during acylation catalysis as detailed in Scheme 3 and the discussion section.

*Overall, we conclude from this section (based on the evidence shown in Figures 7, 8 and 9) that **Triglyme** catalyzes the reaction with the long polymer chains faster than with the short ones. In turn, with **Tet-1** as the catalyst, the shorter polymer chains react faster than the longer ones, which demonstrates that the **Tet-1** catalyst is able to switch the intrinsic reactivity of acylation toward selective functionalization of the shorter chains via size-selective acceleration of the reaction with the shorter chains.*

DISCUSSION

Mechanism of the Size-selective Catalytic Polymer Functionalization

The control reactions executed with simple **Triglyme** and the **Edge-model** demonstrate that not only the triglyme functions of **Tet-1**, but also the cavity of the tetrahedron are important for catalysis. For instance, the slope (= $k_{obs}[cat]_0$) of the rate plot with the **NH_2-POA** substrate increased (Figure 6a) from 7.9 ± 0.9 M^{-1} h^{-1} (R^2 = 0.96) without any additives to 13.0 ± 0.9 M^{-1} h^{-1} (R^2 = 0.97) with simple **Triglyme** (3.4 mM) as the catalyst, demonstrating glyme-catalysis[62] in our system. Next, with **Edge-model** (1.7 mM) as the catalyst, the slope of the rate plot — 13.3 ± 0.7 M^{-1} h^{-1} (R^2 = 0.98) — turned out to be almost identical to the value obtained with **Triglyme**. However, we then observed a very significant jump in the rate plot slope (= $k_{obs}[cat]_0^2$) to 64.9 ± 3.0 M^{-1} h^{-1} (R^2 = 0.99) by utilizing the whole tetrahedron (**Tet-1**, 0.28 mM) as the catalyst. This data is consistent with a mechanism (Scheme 3), where both the glyme functionalities as well as the voluminous cavity of the molecular tetrahedron **Tet-1** actively participate in the size-selective polymer-functionalization mechanism.

Furthermore, from the measured second-order rate dependence on the **Tet-1** concentration, we can conclude that two tetrahedra must be interacting[65] with the polymeric substrate in the rate-determining transition state of the reaction. Thus, based on (i) our kinetic data and (ii) the fact that the solvodynamic diameter of the polymers increases very significantly upon binding to **Tet-1** (see Figures 3, 4, and 10 for corresponding experimental and computational evidence), we propose the mechanism shown in Scheme 3 for the observed catalytic polymer functionalization. In the proposed mechanism, the hydrazone functionalities hydrogen bond (Figure 5c) with functional groups on the polymers and thereby help unfold (see Figure 4 for an MD simulation of this process) the polymer chains to render the amines more reactive: The first **Tet-1** molecule involved in the transition state frees up the amine nucleophile, while the second **Tet-1** frees up the amine-base. At the same time, the triglyme functional groups of **Tet-1** engage in catalysis by stabilizing the tetrahedral intermediates arising during aminolysis. Finally, another amino-group on the polymer acts as a base (freed up by the second equivalent of **Tet-1** bound to the transition state) to deprotonate and break apart the tetrahedral intermediate, which is clearly shown by the observed (Figures 6a, 9a, and 9b) second order rate-dependence on the amine concentration.

The Role of Tet-1's Cavity During Catalysis

Figure 9 provides additional evidence for polymer unfolding taking place thanks to the cavity of the **Tet-1** catalyst. Specifically, we observed (Figure 9b) that an edge of **Tet-1** (**Edge-Model**) leads to an overall *slower* acylation rate than the much smaller **Triglyme** catalyst only for the longer polymeric substrates (**Long-NH_2-POA**). At the same time these two control catalytic systems performed (Figure 9a) at approximately identical rates with the shorter polymer chains (**Short-NH_2-POA**). This difference in catalytic activity is explained (Figure 10) by polymer folding and the formation of relatively small aggregates (Figure 7). Since the longer polymers contain, on average, more amino groups per chain than the shorter ones, polymer folding and aggregate formation occurs to a larger extent with the longer chains. Thus, the bulky **Edge-Model** as the catalyst performs worse as a catalyst for the longer polymers chains only, since the amino-groups occluded inside of the folded/aggregated long polymers can't be approached (Figure 10) effectively by the bulky **Edge-Model** catalyst.

While, these results are in line with what has been observed[66] previously for non-catalytic reactions — for which aggregation has been shown to reduce reaction rates — we have now been able to demonstrate that folding/aggregation-dependent reactivity can be directly influenced by changing the nature of an organocatalyst. Remarkably, with the even bulkier **Tet-1** as the catalyst, the reaction speeds up again (Figure 9b) with the longer polymer chains (**Long-NH_2-POA**) as the substrates. This result is a clear indication that **Tet-1** is able to unfold the polymeric substrates. It further highlights the importance of **Tet-1**'s large cavity, which is lacking in **Edge-Model** and seems to be required for efficient unfolding and catalytic functionalization of the polymeric substrates.

Origin of the Observed Size Selectivity

It is likely that a nanosized catalyst like **Tet-1** can distinguish polymeric substrates of different sizes due to complex, large-section contacts, resembling interactions between biological macromolecules. Such non-local supramolecular recognition is

difficult to achieve with small-molecule catalysts like **Triglyme**, since a small molecule catalyst interacts with reactive groups on the polymers (e.g. amines in our case) mostly in a local fashion. Although a small-molecule catalyst can also form multivalent contacts with its polymeric substrates, it will, in most instances, simply not be able to reach far away sections of a polymeric substrate to enable size-selective functionalization of such large substrates.

As suggested by MD simulations (Figure 4), **Tet-1** interacts with the polymeric substrates in a non-local fashion. Specifically, other amines and carboxylic acids — far away from a reactive amino group on the same polymer — can still influence the interactions between the polymeric substrate and **Tet-1** through hydrogen-bonding networks (see Figure 5c for an example). Therefore, we expect the **Tet-1** catalyst to distinguish different, non-local aspects of a polymer's structure, including (i) polymer length, (ii) the number and types of functional groups present on the polymer, as well as (iii) the positioning of these functional groups. In this work, we now provide evidence (see Figures 7, 8, and 9) for the effect of polymer length on the catalytic rates with **Tet-1** and with small-molecule catalysts. From the kinetic evidence (i.e. the observed second order dependence of the reaction rates on the amine concentration), it is clear that longer polymer chains intrinsically react faster with a small-molecule catalyst like **Triglyme**. However, by switching to **Tet-1** as the catalyst, this intrinsic reactivity can be partially reversed. Overall, by providing initial evidence for size selectivity with polymeric substrates, we lay the foundation to further investigate the complex factors governing polymerization catalysis for selective post-synthetic polymer modification reactions. Some key factors we identified thus far include:

(i) The thermodynamic stability of the [**polymer@Tet-1**] complex. As has been established for classical enzyme kinetics, where the binding strength of the substrate with the enzyme has to be[61] "just right" and neither "too tight" nor "too loose" for efficient catalysis, we find (Figure 5b) that weaker binding of the substrate can indeed enhance the catalytic activity of our PSPM catalyst.

(ii) The availability of a large cavity in the catalyst, which is able to unfold the polymeric substrates. Notably, a simple edge of the tetrahedron (**Edge-model**) does not perform nearly as efficiently as the full tetrahedron.

(iii) A reactive complexation geometry, in which the polymers are not only partially unfolded (and threaded through the cavity of the catalyst), but also placed in close proximity to the catalytic triglyme units on the tetrahedron.

(iv) The ability of the catalyst to free up at least two amino groups on a polymer, the first one acing as the nucleophilic substrate for acylation, and the second one as the amine base needed for efficient deprotonation of the tetrahedral acylation intermediates.

(v) Aggregation (Figure 7) of the polymer chains. While prior work has shown[66-67] that aggregation reduces the reaction rates for non-catalytic reactions, we discovered that for our system aggregation and folding effects are strongly catalyst dependent. For example, folding/aggregation of the longer polymer chains significantly reduces (Figure 9b) the reactivity of the long chains with the **Edge-model** catalyst. At the same time, aggregation effects are not strong enough (Figure 9b) to slow down the **Tet-1**-catalyzed reaction with the long polymers in comparison with the small **Triglyme** catalyst. Rather, our results shown in Figure 9 clearly indicate that the observed size selectivity is caused by selective *acceleration* of **Tet-1**'s reaction with the short polymers.

Overall, our findings (especially the relative rates shown in Figure 9) clearly demonstrate (Figure 10) that aggregation/folding effects can mostly be overcome by threading polymers through the cavity of a porous catalytic tetrahedron, which leads to partial unfolding (Figure 4) of the polymer chains.

Conclusions

In conclusion, we demonstrated the concept of post-synthetic selective polymer modification operating in complex mixtures of polymeric substrates. Our reaction proceeds with size selectivity in the presence of a hydrazone-linked tetrahedron with wide openings as the catalyst, in sharp contrast to the results observed with small-molecule catalysts. This conclusion is supported by (i) distinct differences in the overall solvodynamic radii of the of the polymeric products, (ii) by a significant alteration in the relative diffusion constants for the functionalized polymers compared to the unfunctionalized ones, as well as (iii) by rate constants measured separately for the shorter and longer polymer chains. Our findings extend the scope of catalyst-controlled size selectivity to large substrates for post-synthetic polymer-functionalization reactions, applied to polydisperse polymer mixtures. Our size-selective, catalytic approach represents a promising avenue to create next-generation polymers.

EXPERIMENTAL PROCEDURES

Resource Availability

Lead Contact

Further information and requests for resources and reagents should be directed to and will be fulfilled by the Lead Contact, Severin T. Schneebeli (severin.schneebeli@uvm.edu).

Materials Availability

Tet-1 generated in this study will be made available on request, but we may require a payment and/or a completed Materials Transfer Agreement if there is potential for commercial application.

Data and Code Availability

Raw data for (i) compound characterization (^{1}H and ^{13}C (^{1}H) NMR, ^{1}H-^{1}H NOESY NMR, DOSY ^{1}H NMR, HRMS, IR, and DLS), (ii) the ^{1}H NMR titrations, and (iii) the ^{1}H NMR-based kinetic measurements are available freely from the Mendeley Data Repository at http://dx.doi.org/10.17632/vn92mr6z69.1. The MD trajectory of **NH_2-POA** is available freely from the Mendeley Data Repository at http://dx.doi.org/10.17632/k4nb4z3ff5.1. The MD trajectory of the [**NH_2-POA@Tet-1**] complex is available freely from the Mendeley Data Repository at http://dx.doi.org/10.17632/69x74bkdb5.1
.

General Synthetic Procedures

Chemical synthesis was performed as detailed in the Supplemental Experimental Procedures section. See Figures S30–S64 for the ^{1}H and ^{13}C (^{1}H) NMR spectra of all products and key synthetic intermediates created as well as Figure S65 for the FTIR spectrum of **NH_2-POA** and Figure S66 for the dynamic light scattering (DLS) characterization data for **NH_2-POA**, **Short-NH_2-POA**, and **Long-NH_2-POA**.

Synthesis of Tet-1

Syn-**7** (0.274 g, 0.208 mmol) was dissolved in 350 mL dry CH_2Cl_2, and the solution was degassed with argon. Next, terephthalaldehyde (41.9 g, 0.312 mmol) and high performance liquid chromatography (HPLC) grade TFA (24 μL, 0.313 mmol) were added consecutively, and the reaction mixture was stirred at room temperature under an argon atmosphere. After 48 h, the acid was neutralized with a saturated aqueous sodium bicarbonate solution (10 mL), the organic layer was separated, and the aqueous phase extracted with additional CH_2Cl_2 (30 mL). Finally, the combined organic extracts were washed with brine, dried over anhydrous Na_2SO_4, filtered, and concentrated under reduced pressure. The crude product was purified by size exclusion chromatography over polystyrene beads (200–400 mesh) with CH_2Cl_2 as the eluent to afford **Tet-1** as an orange-yellow solid.

*Yield and Characterization Data for **Tet-1***

Yield: 0.242 g (80%); ^{1}H NMR (500 MHz, CD_2Cl_2): δ 11.08 (s, 12H), 8.26 (s, 12H), 7.99 (s, 12H), 7.84 (s, 24H), 6.64 (s, 12H), 4.33 (t, *J* = 6.6 Hz, 24H), 3.89 (s, 36H), 3.63 – 3.44 (m, 168H), 3.29 (s, 36H), 2.16 – 2.08 (m, 24H), 1.88 (m, 24H), 1.67 (s, 36H); ^{13}C (^{1}H) NMR (125 MHz, CD_2Cl_2): δ 162.0, 161.2, 157.9, 146.6, 136.5, 135.7, 135.5, 135.1, 128.3, 124.6, 113.7, 96.4, 72.4, 71.1, 71.0, 71.0, 71.0, 70.9, 70.8, 70.1, 59.1, 56.3, 26.9, 26.9, 19.0; HRMS (ESI+) *m/z*: $[M + 5H]^{5+}$ calcd 1170.9964, found 1170.9982.

Synthesis of NH_2-POA

Poly(isobutylene-*alt*-maleic anhydride) ($\overline{M}_w$ = 6 kDa, 0.500 g, 0.083 mmol of polymer, 3.237 mmol of anhydride units) was dissolved in anhydrous *N*,*N*-dimethylformamide (DMF, 1.0 mL) while heating at 85 °C. In a different vial, 1-aminooctane (0.378 g, 2.925 mmol) was dissolved in anhydrous DMF (1.0 mL) at the same temperature. Next, the 1-aminooctane solution was added to the polymer solution and the reaction mixture was stirred at 89 °C for 24 h. The temperature was then increased to 125 °C for 2 h under a stream of dry N_2 to remove the water formed in the condensation reaction. Finally, the temperature was increased further to 170 °C and the reaction mixture stirred for another hour at that temperature under a stream of dry N_2 to obtain an orange oil. Next, the crude sample (0.740 g, 0.0706 mmol) was dissolved in anhydrous DMF (2.0 mL), followed by addition of excess 1,6-diaminohexane (75 mg, 0.64 mmol) and the reaction mixture was heated at 71 °C for 45 h. The temperature was increased to 95 °C and the solvent was evaporated over dry N_2 for 2 h. Finally, the crude reaction mixture was purified by size exclusion chromatography over polystyrene beads (200–400 mesh) with CH_2Cl_2 as the eluent to afford **NH_2-POA** as a viscous yellow oil. Based on elemental analysis (*vide infra*), the percentages (defined in Scheme 2) of repeating units a, b, and c were (with 2.2% crystal water): a = 57.8%, b = 17.8%, and c = 22.2%.

*Yield and Characterization Data for **NH_2-POA***

Yield: 0.773 g (73%); ^{1}H NMR (500 MHz, CD_2Cl_2): δ 3.70–2.10 (broad m, ~102H), 1.80–0.60 (broad m, ~490H); IR (film): ν = 3316 (broad, amide N-H stretching and carboxylic acid O-H stretching), 2928, 2859, 1694 (carbonyl C=O stretching); DOSY ^{1}H NMR (500 MHz, $CDCl_3$, polystyrene standard, see Figure S5 for the calibration curve): $\overline{M}_w$ = 6.3 kDa; Dynamic light scattering (DLS, CH_2Cl_2): Polydispersity index (PDI) = 1.5; Anal. calcd (mass %) for $(C_{16}H_{29}NO_3)_{12.1}$ $(C_{22}H_{43}N_3O_2)_{3.7}$ $(C_{24}H_{46}N_2O_2)_{4.7} \cdot 0.5\ H_2O$: C, 67.77; H, 10.84; N, 6.39. Found: C, 67.80; H, 11.22; N, 5.99.

Isolation of Short- and Long-NH_2-POA

Analytical samples of the shortest (**Short-NH_2-POA**, $\overline{M}_w$ (DOSY) = 2.6 kDa) and longest (**Long-NH_2-POA,** $\overline{M}_w$ (DOSY) = 9.9 kDa) polymer chains in the **NH_2-POA** sample were obtained by running a second size exclusion column of **NH_2-POA** (0.272 g) over polystyrene beads (200–400 mesh) with CH_2Cl_2 as the eluent. Collection of the compound eluting first (at 43 minutes) resulted in **Long-NH_2-POA**, while collection of the fractions eluting last (at around 80 minutes) resulted in **Short-NH_2-POA**. Based on elemental analysis, the percentages (defined in Scheme 2) of repeating units a, b, and c were: a = 50.9%, b = 12.0%, and c = 34.7% (with 2.4% crystal water) for **Short-NH_2-POA** and a = 48.7%, b = 5.0%, and c = 43.6% (with 2.7% crystal water) for **Long-NH_2-POA.** The molecular weights of the different polymer samples were determined (see Figures S4–S6, as well as Tables S1 and S2) with dynamic light scattering (DLS) as detailed in the Supplemental Experimental Procedures section.

*Yield and Characterization Data for **Short-NH_2-POA***

Yield: 0.046 g (41%, based on the total amount of **NH_2-POA** added to the second size-exclusion column); ^{1}H NMR (500 MHz, CD_2Cl_2): δ 3.70–2.30 (broad m, ~46H), 2.20–0.50 (broad m, ~220H); DOSY ^{1}H NMR (500 MHz, $CDCl_3$, polystyrene standard, see Figure S5 for the calibration curve): $\overline{M}_w$ = 2.6 kDa; DLS (CH_2Cl_2): PDI = 1.3; Anal. calcd (mass %) for $(C_{16}H_{29}NO_3)_{4.6}(C_{22}H_{43}N_3O_2)_{1.1}(C_{24}H_{46}N_2O_2)_{3.1}\cdot 0.2\ H_2O$: C, 68.14; H, 10.96; N, 6.30. Found: C, 68.13; H, 11.09; N, 6.33.

*Yield and Characterization Data for **Long-NH_2-POA***

Yield: 0.103 g (25%, based on the total amount of **NH_2-POA** added to the second size-exclusion column); ^{1}H NMR (500 MHz, CD_2Cl_2): δ 3.60 – 2.20 (broad m, ~162H), 1.70–0.70 (broad m, ~854H); DOSY ^{1}H-NMR (500 MHz, $CDCl_3$, polystyrene standard, see Figure S5 for the calibration curve): $\overline{M}_w$ = 9.9 kDa; DLS (CH_2Cl_2): PDI = 1.5; Anal. calcd (mass %) for $(C_{16}H_{29}NO_3)_{16.1}(C_{22}H_{43}N_3O_2)_{1.6}(C_{24}H_{46}N_2O_2)_{14.4}\cdot 0.9\ H_2O$: C, 68.34; H, 11.01; N, 6.05. Found: C, 68.36; H, 11.34; N, 5.77.

Sample Preparation and Measurements of Rate Constants

For all kinetic measurements, stock solutions of all reagents in CD_2Cl_2 were prepared in advance and used promptly. The stock solutions were stored at –10 °C in sealed vials under an argon atmosphere. All volumetric measurements were performed with Rainin Positive Displacement (MR-10, -100, -1000) micropipettes, which are optimized for organic solvents with low vapor pressures like CD_2Cl_2. The concentrations of reagents in the stock solutions were calibrated by ^{1}H NMR integration and comparison of the integrals with the integral of 1,2,4,5-tetrabromobenzene (TBB) as the internal standard. For each time-dependent ^{1}H NMR experiment, the active ester (NDB, 5.1 mM) was added last to the reaction mixtures and the addition time of NDB is reported as the start time of the experiments. The progress of the aminolysis reactions was monitored by integrating (Figures S13–S26) the ^{1}H-NMR resonance at 6.9 ppm, which corresponds to *p*-nitrophenol formed (Scheme 3) upon aminolysis of the NDB active ester. Absolute concentrations of the *p*-nitrophenol in all the samples were obtained by comparing the integrations of the *p*-nitrophenol resonances to the integrations of the internal TBB standard. Finally, the concentrations of the remaining amino groups ([amine]) on the **NH_2-POA** polymers were calculated for each time point by subtracting the amount of *p*-nitrophenol formed from the initial amine concentrations ($[amine]_0$). With the 1.8 mg of polymer sample used for each kinetic experiment, the initial amine concentrations were, approximately: 1.8 mM for **NH_2-POA**, 1.2 mM for **Short-NH_2-POA**, and 0.5 mM for **Long-NH_2-POA**.

DOSY ^{1}H NMR Analysis of Polymer Acylation Experiments

For the DOSY ^{1}H NMR analysis of the polymer acylation reactions, two reaction mixtures were prepared in separate NMR tubes, and reaction progress was monitored by following the ^{1}H NMR integrations of the *p*-nitrophenol resonances at 6.9 ppm in both samples. Both reactions were then equalized as described in detail in Figure 7 (caption) at 24% conversion. In order to minimize further reaction progress while recording the DOSY ^{1}H NMR spectra, the DOSY ^{1}H NMR spectra were recorded with 30 increments in 20–25 minutes. The diffusion delay Δ, was set to 60 ms, with the diffusion gradient length δ at 3 ms, which required 32 scans for each gradient-strength measurement.

MD Simulations

In order to verify our proposed model for the observed kinetic behavior of **Tet-1**, we employed 800-ns MD simulations with the OPLS3e[68] force field in explicit CH_2Cl_2 solvent. The MD simulations (i) explain the outcome of the DOSY ^{1}H-NMR spectra shown in Figure 3. Specifically, the **NH_2-POA** polymer unfolds upon binding to **Tet-1** and it increases (Figure 4) in size during that process. (ii) The MD simulations also shed light on the alteration of the supramolecular interactions present within the polymer upon binding to **Tet-1**. As shown in the supplemental information (Figure S29), the number of intramolecular hydrogen bonds folding up the polymer decreases by binding to **Tet-1** as these intra-polymer hydrogen bonds get replaced with hydrogen bonds formed between **Tet-1** and the polymer.

Model Preparation

All models were constructed using the Maestro program (2018-2 release). **Tet-1** and [**NH_2-POA@Tet-1**] systems were simulated in periodic simulation boxes of ~121 × 121 × 121 Å^3 and ~67 × 67 × 67 Å^3, respectively, with CH_2Cl_2 molecules as the solvent. Each construct went through minimization, equilibration, and either 100-ns, 250-ns, or 800-ns MD production stages, depending on convergence speed. At least two replicas with differing random seeds were run for all simulations.

Simulation Setup and Analysis

Each model was simulated in the NPT ensemble (300 K, 1 atm, Martyna-Tuckerman-Klein coupling scheme). All simulations were performed in the Maestro-Desmond program (GPU version 5.4) with a time step of 2 fs. The Ewald technique was used for the electrostatic calculations. The Van der Waals and short-range electrostatics were cut off at 9 Å. Hydrogen atoms were constrained using the SHAKE algorithm. MD trajectories were analyzed using in-house python scripts and the Schrödinger (2018-2 release) API.

SUPPLEMENTAL INFORMATION

Document S1. Supplemental Experimental Procedures, Figures S1–S66, as well as Tables S1 and S2.

Video S1. MD Trajectories Comparing the Structure of a Free NH2-POA Polymer Chain with the Same Polymer in Complex with Tet-1

ACKNOWLEDGMENTS

We thank B. O Rourke for high-resolution mass spectrometry. The synthesis of **Tet-1** and execution of the initial kinetic experiments was supported by the National Science Foundation (NSF, Grant CHE-1609137 awarded to S.T.S), while the kinetic

experiments with the **Short-** and **Long-NH_2-POA** polymers were supported by an NSF CAREER Award (Grant CHE-1848444 awarded to S.T.S). Partial support for the computational work was also provided by the ACS Petroleum Research Fund (Grant 58219-DNI6) and the National Institutes of Health (Grant NIH-R01GM129431) awarded to JL, as well as by the National Institutes of Health (Grants S10-OD018126 and P30-GM118228 supporting the UVM Mass Spectrometry facilities). The graphics processing units used for the modeling were provided by NVIDIA via the GPU grant program.

AUTHOR CONTRIBUTIONS

S.T.S. and J.L. conceived and guided the project, obtained funding, discussed the experimental and computational results, and wrote the paper together with M.S. M.S., K.T.M., D.R.M., N.D., S.C.R., J.P.C., and K.E.M. performed the experiments and analyzed the experimental data. K.T.M. performed the MD simulations and analyzed the computational results. M.I. assisted M.S. with the DOSY ^{1}H-NMR experiments. Y.S. and A.R.B. assisted M.S. with the DLS measurements. All authors discussed the results and revised the paper.

DECLARATION OF INTERESTS

The authors have no competing financial interests to declare. N.D. is currently a graduate student at Yale University (New Haven, CT). K.E.M. is currently employed at the University of North Carolina, Asheville (Asheville, NC). S.C.R is currently a postdoctoral researcher at the University of Southern Mississippi (Hattiesburg, MS). J.P.C. is currently employed as a Scientist at Integrity Industrial Ink Jet Integration, *LLC* (West Lebanon, NH). However, N.D., K.E.M., S.C.R., and J.P.C performed the work for this paper at the University of Vermont (Burlington, VT). Some of the authors have also filed a provisional patent application related to this work.

LEAD CONTACT STATEMENT

Further information and requests for resources and reagents should be directed to and will be fulfilled by the Lead Contact, Severin T. Schneebeli (severin.schneebeli@uvm.edu).

Figure 1. Substrate-selective Catalysis — From Small-molecule to Polymeric Substrates

(A) Examples of prior work in the size-selective catalysis arena with small-molecule substrates.

(B) We extend the concept of size-selective catalysis to larger substrates with a hydrazone-linked molecular tetrahedron as the organocatalyst, which can size-selectively modify a polydisperse mixture of polymer chains. Catalysts are shown in green, reactive substrates and products in orange, unreactive substrates in yellow-orange, and reagents in blue/black. All structures are shown approximately on the same scale and the polymer chains are illustrated schematically in their fully extended conformations. Please note that — as detailed in the results/discussion sections — the longer polymer chains have a tendency to not only fold, but also aggregate more than the shorter ones, which can explain the catalyst's selectivity towards the shorter polymer chains.

Figure 2. Comparison of Tetrameric Hydrazone-linked Molecular Cages

(A) C_{2d}-symmercial hydrazone cage reported[47] by Warmuth and coworkers.

(B) The T_d-symmetrical hydrazone tetrahedron reported in this work. Its wide openings allow it to act as a size-selective catalyst for post-synthetic polymer modification (PSPM). Molecular models of both cages were minimized with the OPLS3[48] force field. Color scheme: C = green, polar H = white, N = blue, O = red.

Scheme 1. Synthesis of the Hydrazone-linked Molecular Tetrahedron Tet-1

Reagents and conditions: (i) BCl_3, CH_2Cl_2; (ii) Br-C_4H_8-Triglyme, K_2CO_3, DMF, Δ; (iii) MeOH, H_2SO_4, Δ; (iv) H_2NNH_2, MeOH, H_2O, Δ.

Scheme 2. Synthesis of an Amine-functionalized Polymeric Substrate for Size-selective Catalysis
Reagents and conditions: (i) H_2N-*n*-C_8H_{17}, DMF, Δ; (ii) H_2N-*n*-C_6H_{12}-NH_2, DMF, Δ. Based on elemental analysis and the $\overline{M}_w$ (6.3 kDa), the average number of repeating units a, b, and c were: a = 12.1, b = 3.7, and c = 4.7.

Figure 3. ^{1}H DOSY and ^{1}H-^{1}H NOESY NMR Spectra Demonstrate Complex Formation and Threading of the Polymers Through the Cavity of the Tet-1 Catalyst
(A–C) Partial ^{1}H DOSY NMR spectra (500 MHz, CD_2Cl_2, 298 K) of (A) **Tet-1** (0.28 mM), (B) a mixture of **Tet-1** (0.28 mM) and **NH_2-POA** (3.0 mg mL^{-1}; 0.45 mM), as well as (C) pure **NH_2-POA** (3.0 mg mL^{-1}; 0.45 mM). The spectra show a decrease of the diffusion constants for both **NH_2-POA** and **Tet-1** upon mixing. This finding establishes complex formation between the two compounds. The diffusion constant of the solvent ($CHDCl_2$) resonance at 5.32 ppm remained constant (32.5 x 10^{-10} m^2 s^{-1} in all cases, see Figure S3), indicating that the viscosities of the NMR solutions were not affected significantly by the presence of the polymers at the low concentrations employed.
(D) Partial ^{1}H-^{1}H NOESY NMR spectrum (500 MHz, CD_2Cl_2, 298 K) of **Short-NH_2-POA** (3.0 mg mL^{-1}) in complex with **Tet-1** (0.28 mM). **Short-NH_2-POA** represents the shorter chains ($\overline{M}_w$ = 2.6 kDa) of the **NH_2-POA** polymer sample, which were isolated (see the experimental procedures section) by running an additional size-exclusion column on parts of the original **NH_2-POA** sample. NOE cross peaks between the aliphatic polymer resonances *Poly-aliphatic* and signals corresponding to **Tet-1** are circled. Notably, a NOE cross peak between *Poly-aliphatic* and the *c* protons on **Tet-1** (pointing inward) is observed, which is consistent with the **NH_2-POA** polymers threading through the cavity of **Tet-1**. An analogous NOESY spectrum has been obtained (see Figure S7) for the longer chains in **NH_2-POA**, i.e. **Long-NH_2-POA** ($\overline{M}_w$ = 9.9 kDa), which shows similar (although slightly weaker) NOE cross peaks.

Figure 4. MD Simulations Showing an NH_2-POA Polymer Chain Unfolding when Binding to Tet-1
The MD simulations help explain the increase of the polymer's solvodynamic diameter, which is observed (Figure 3B) upon complexation with **Tet-1** by ^{1}H DOSY NMR spectroscopy.
(A) Time-average bar-charts showing the radius of gyration (rgyr) of the **NH_2-POA** polymer chain by itself (pattern-free bar) and in complex (patterned bar) with **Tet-1**. Error bars represent standard deviations. The time-averages and standard deviations were calculated from the last 400 ns of 800-ns MD simulations in explicit solvent.
(B and C) Representative snapshots of 800-ns MD simulations of **NH_2-POA** by itself (B) and **NH_2-POA** threaded through the cavity of **Tet-1** (C). The solvent (CH_2Cl_2) is hidden for clarity.

Figure 5. Long-NH_2-POA Binds Stronger to Tet-1 than Short-NH_2-POA but the Short Polymers De-complex Faster
(A) Stacked partial ^{1}H NMR spectra (500 MHz, CD_2Cl_2, 298 K) demonstrating how key **Tet-1** and polymer resonances change upon titration of **Short-NH_2-POA** into a 0.28 mM solution of **Tet-1**. See Figures S11 for the titration of **Tet-1** with itself (Figure S11) and Figure S12 for the titration of **NH_2-POA** with itself.
(B) Titration curves fitted to a 1:1 binding model in the intermediate-slow NMR exchange regime for threading of both **Short-** and **Long-NH_2-POA** into the cavity of **Tet-1.** While the longer polymer chains bind stronger to **Tet-1** (which leads to weaker catalysis with the longer chains as illustrated in Figure 9D), the shorter polymer chains de-thread faster (with an off-rate, k_{off}, nearly three-times as fast as for the longer polymers). K_a = Complex association constants. The titration curves were fit with a custom python script, making use of the LineshapeKin 4.0 NMR simulation software[58] in combination with the curve-fit algorithm implemented in the SciPy 0.18 package[59] with the trust region reflective (TRF) algorithm. Error bars represent standard deviations calculated from the covariance matrix of the best fit obtained with the SciPy curve-fit algorithm. See Figures S8–S9 for a full comparison of the experimental and predicted spectra and the Supplemental Experimental Procedures section for the custom python code used to implement the parameter fitting.
(C) Zoomed-in, representative snapshot from the 800-ns MD simulation of the [**NH_2-POA@Tet-1**] complex (see Figure 4C for a zoomed-out view). The snapshot shows that the threaded polymer chains preferentially pass by the side of the aromatic linkers in **Tet-1**. We hypothesize that classical[55] aromatic ring-current effects operating in this binding geometry are primarily responsible for the observed downfield[54] shifts, which occur (Figure 5A) for the polymer resonances in the range of 3.05–2.55 ppm upon complexation with **Tet-1**.

Figure 6. Evidence of Tet-1's Catalytic Activity for Functionalizing NH_2-POA Polymers
Plots of the inverse total amine concentration ($[amine]^{-1}$) *vs.* time. The fact that these plots are linear demonstrates that the reactions are all 2nd order in the amine concentration. The kinetic experiments were carried out in 600 µL of CD_2Cl_2 at 298 K using an initial amine concentration of 1.8 mM, with an excess (5.1 mM) of the active ester 4-nitrophenyl-3,5-dinitrobenzoate (NDB) in the presence of one of the following catalysts: 0.28 mM **Tet-1** (green circles); 1.7 mM **Edge-Model** (red triangles); 3.4 mM **Triglyme + Control** (gray squares); no catalytic additives (blue triangles).

Table 1. Observed Rate Constants (k_{obs}) for the NH_2-POA Polymer Acylation Reactions

Organocatalyst	k_{obs}[a]	$\bar{m}$[b]
Tet-1 (0.28 mM)[c]	(8.3 ± 0.9) x 10^8 M^{-3} h^{-1}	3.0 ± 0.2
Edge-model (1.7 mM)[c]	(7.8 ± 0.6) x 10^3 M^{-2} h^{-1}	2.0 ± 0.1
Control + **Triglyme** (3.4 mM each)[c]	(3.6 ± 0.3) x 10^3 M^{-2} h^{-1}	2.0 ± 0.1
Triglyme (3.4 mM)[d]	(3.8 ± 0.3) x 10^3 M^{-2} h^{-1}	1.9 ± 0.1
No Organocatalyst[c]	(7.9 ± 0.9) x 10^0 M^{-1} h^{-1}	1.5 ± 0.1

[a]Observed rate constants (defined in Equations 1–3). Data are represented as mean ± SEM.
[b]Average number of acylated amines per polymer chain after 48 h of reaction time. Data are represented as mean ± SEM.
[c]See Figure 6 for the corresponding rate-plots with **Tet-1**, **Edge-model**, as well as **Control** + **Triglyme**.
[d]See Figure S23D for the corresponding rate-plot with only **Triglyme** as the catalyst.

Figure 7. Solvodynamic Diameters of the NH_2-POA Polymers Provide Evidence for Size Selectivity in the Polymer Mixture

The **NH_2-POA** polymers contain (Scheme 2) both NH_2 and COOH functional groups. In the non-polar CD_2Cl_2 solvent used for the acylation reactions, these functionalities form strong hydrogen bonds, that are required (Figure 5C) in order for **Tet-1** to bind to the polymeric substrates. In addition, the hydrogen-bonding capabilities of the polymers also induce some aggregation of the polymers. Overall, longer polymer chains have a statistically higher chance to form aggregated structures, since they contain a larger number of NH_2 and COOH functional groups on average. When the NH_2 groups on the polymers are acylated with NDB, some of the [-NH_2···HOOC-]-hydrogen bonds disappear, which reduces aggregation of the polymers. Now, if longer polymers get acylated the most, the observed reduction in aggregation will be stronger than if shorter polymer chains get acylated the most. From the measured solvodynamic diameters we observe a smaller reduction in average size (from 4.9 to 4.5 nm) for the reaction executed with **Tet-1** as the catalyst than for the control reaction (4.9 nm to 2.8 nm). This data therefore indicates that shorter polymer chains got acylated the fastest with **Tet-1** as the catalyst, while longer polymer chains got acylated preferentially in the control reaction. Data are represented as mean ± SEM. **Tet-1** (0.28 mM) was added to measure the solvodynamic diameter of the dissolved **NH_2-POA** starting material to obtain a more accurate size-comparison with the product samples, which also contained **Tet-1** in the same concentration.

Figure 8. Additional Evidence for Size-selectivity in the Acylation Reactions of the Polymer Mixture Based on Relative Diffusion Constants

(A and B) A direct comparison of the relative diffusion constants for the functionalized polymers with the average diffusion constants of all the polymer chains (both functionalized and unfunctionalized). (A) With **Tet-1** as the catalyst. (B) Control reaction with **Triglyme** + **Control** as the catalysts. The average diffusion constant of the functionalized polymers was measured via the diffusion constant of the distinct ^{1}H-NMR resonance at 8.82 ppm, which corresponds to the *ortho*-protons (resonance *X*) of the 3,5-dinitrobenzamide units attached to the functionalized polymers. The average diffusion constant of all polymer chains was determined from the diffusion constant of the broad ^{1}H NMR resonances between 0.8 to 1.4 ppm, which correspond to the aliphatic protons of the polymer chains. All reactions were run to 24% conversion and all ^{1}H DOSY NMR spectra were obtained for reaction mixtures "equalized" in the following manner: (A) For the functionalization reaction catalyzed by **Tet-1** (0.28 mM), we added **Triglyme** (3.4 mM) and **Control** (3.4 mM) just before recording the DOSY ^{1}H-NMR spectrum. (B) For the control reaction catalyzed by **Triglyme** (3.4 mM) + **Control** (3.4 mM), we added **Tet-1** (0.28 mM), again just before recording the DOSY ^{1}H-NMR spectrum.

Figure 9. The Rate Constants (k_{obs}) Measured for Isolated Short and Long Polymer Samples Confirm that Tet-1 is a more active catalyst for Shorter Polymer Chains

(A and B) Plots of the inverse total amine concentration ([amine]$^{-1}$) vs. time for **Short-NH_2-POA** (A) and **Long-NH_2-POA** (B). The kinetic experiments were carried out in 600 μL of CD_2Cl_2 at 298 K using an initial amine concentration of 1.2 mM for **Short-NH_2-POA** and 0.5 mM for **Long-NH_2-POA** with an excess (5.1 mM) of the active ester 4-nitrophenyl-3,5-dinitrobenzoate (NDB) in the presence of one of the following catalysts: 0.28 mM **Tet-1** (green circles); 1.7 mM **Edge-Model** (red triangles); 3.4 mM **Triglyme** + **Control** (gray squares).

(C) Proposed model (schematic) explaining why the **Tet-1** catalyst *reacts* faster with the shorter polymer chains, while it *binds* stronger to the substrates (but not to the transition states) with longer polymer chains. $\Delta G^{\ddagger}$ (Long) = Activation Gibbs free energy with **Long-NH_2-POA**; $\Delta G^{\ddagger}$ (Short) = Activation Gibbs free energy with **Short-NH_2-POA**; ΔG_b (Long) = Binding Gibbs free energy with **Long-NH_2-POA**; ΔG_b (Short) = Binding Gibbs free energy with **Short-NH_2-POA**.

Table 2. Observed Rate Constants (k_{obs}) for the Acylation Reactions of the Individual Short- and Long-NH_2-POA Polymers

Organocatalyst	k_{obs}[a, b] with **Short-NH_2-POA**	k_{obs}[a, c] with **Long-NH_2-POA**
Tet-1 (0.28 mM)	(2.9 ± 0.4) x 10^9 M^{-3} h^{-1}	(1.9 ± 0.3) x 10^9 M^{-3} h^{-1}
Edge-model (1.7 mM)	(6.8 ± 0.6) x 10^4 M^{-2} h^{-1}	(4.6 ± 0.6) x 10^4 M^{-2} h^{-1}
Control + **Triglyme** (3.4 mM each)	(3.4 ± 0.2) x 10^4 M^{-2} h^{-1}	(4.3 ± 0.4) x 10^4 M^{-2} h^{-1}

[a]Observed rate constants (defined in Equations 1 and 2). Data are represented as mean ± SEM.
[b]See Figure 9A for the corresponding rate-plots with the **Short-NH_2-POA** polymer sample.
[c]See Figure 9B for the corresponding rate-plots with the **Long-NH_2-POA** polymer sample.

Scheme 3. Proposed Catalytic Cycle for Tet-1-catalyzed Acylation of NH_2-POA Polymers

The tetrahedral cage catalyst **Tet-1** (i) helps to unfold (see Figures 3, 4, and 10 for evidence) the polymeric substrates, which frees up the amino groups on the polymers for acylation and base catalysis. In addition, **Tet-1** (ii) utilizes its 12 peripheral triglyme units to stabilize the tetrahedral aminolysis intermediates, while (iii) an internal amino group (freed up by a second equivalent of **Tet-1**) functions as the base to deprotonate the intermediate. The fact that the amines also act as a base in the mechanism results in the observed second order rate-dependence on the amine-concentration. The two **Tet-1** cages bound to the rate-determining transition state lead to the observed (see Figure S27A) second order rate-dependence on the **Tet-1** concentration.

Figure 10. Tet-1's Ability to Unfold the Polymer Chains Explains the Relative Acylation Rates Observed with Long-NH_2-POA with the Three Different Catalysts

Triglyme (3.4 mM) acts (Figure 9B) as a more effective catalyst than **Edge-model** (1.7 mM) for the **Long-NH_2-POA** substrates, while for the **Short-NH_2-POA** substrates both of these catalytic systems perform (Figure 9A) at approximately equal rates. This reactivity trend is explained by polymer folding/aggregation (Figure 7) which occurs preferentially for the longer polymers, which contain more amino groups per chain on average. Remarkably, with the even larger **Tet-1** as the catalyst, the acylation reaction speeds up again for the long polymers. This finding indicates that the large cavity of **Tet-1** can unfold (see Figures 3 and 4 for additional evidence) the polymeric substrates to free up the amines on the polymeric substrates.

Video S1. MD Trajectories Comparing the Structure of a Free NH_2-POA Polymer Chain with the Same Polymer in Complex with Tet-1

Both MD trajectories shown in the video were run for 800-ns with the OPLS3e[68] force field in explicit CH_2Cl_2 solvent, which has been hidden for clarity. These trajectories qualitatively show that, when the polymer chain is free in solution (left trajectory), the polymer chain adopts a more folded conformation, driven by intramolecular hydrogen bonding. When the same polymer chain is in complex with **Tet-1** (right trajectory), it unfolds due to the shape of the cavity as well as due to the formation of new intermolecular hydrogen bonds between the **NH_2-POA** polymer's sidechains and the catalyst's (**Tet-1**'s) hydrazone units. These phenomena are quantified in Figure 4A.

REFERENCES

1. Breslow, R. (1982). Artificial enzymes. Science *218*, 532–537.
2. Trinh, T.; Liao, C.; Toader, V.; Barlog, M.; Bazzi, H. S.; Li, J.; Sleiman, H. F. (2018). DNA-imprinted polymer nanoparticles with monodispersity and prescribed DNA-strand patterns. Nat. Chem. *10*, 184–192.
3. For a review on supramolecular catalysis with metalated hosts see: Brown, C. J.; Toste, F. D.; Bergman, R. G.; Raymond, K. N. (2015). Supramolecular catalysis in metal-ligand cluster hosts. Chem. Rev. *115*, 3012–3035.
4. Mahata, K.; Frischmann, P. D.; Würthner, F. (2013). Giant electroactive M_4L_6 tetrahedral host self-assembled with Fe(II) vertices and perylene bisimide dye edges. J. Am. Chem. Soc. *135*, 15656–15661.

5. For a review on artificial enzyme mimetics see: Raynal, M.; Ballester, P.; Vidal-Ferran, A.; van Leeuwen, P. W. (2014). Supramolecular catalysis. Part 2: artificial enzyme mimics. Chem. Soc. Rev. *43*, 1734–1787.

6. Fang, Y., et al. (2019). Catalytic reactions within the cavity of coordination cages. Chem. Soc. Rev. *48*, 4707–4730.

7. Pappalardo; Puglisi; Trusso, S. (2019). Catalysis inside supramolecular capsules: recent developments. Catalysts *9*, 630.

8. Lewandowski, B., et al. (2013). Sequence-specific peptide synthesis by an artificial small-molecule machine. Science *339*, 189–193.

9. Deutman, A. B.; Cantekin, S.; Elemans, J. A.; Rowan, A. E.; Nolte, R. J. (2014). Designing processive catalytic systems. Threading polymers through a flexible macrocycle ring. J. Am. Chem. Soc. *136*, 9165–9172.

10. Gianneschi, N. C.; Cho, S. H.; Nguyen, S. T.; Mirkin, C. A. (2004). Reversibly addressing an allosteric catalyst in situ: catalytic molecular tweezers. Angew. Chem. Int. Ed. *43*, 5503–5507.

11. Yoshizawa, M.; Tamura, M.; Fujita, M. (2006). Diels-Alder in aqueous molecular hosts: unusual regioselectivity and efficient catalysis. Science *312*, 251–254.

12. Pluth, M. D.; Bergman, R. G.; Raymond, K. N. (2007). Acid catalysis in basic solution: a supramolecular host promotes orthoformate hydrolysis. Science *316*, 85–88.

13. Han, X.; Xia, Q.; Huang, J.; Liu, Y.; Tan, C.; Cui, Y. (2017). Chiral covalent organic frameworks with high chemical stability for heterogeneous asymmetric catalysis. J. Am. Chem. Soc. *139*, 8693–8697.

14. Jiao, J.; Li, Z.; Qiao, Z.; Li, X.; Liu, Y.; Dong, J.; Jiang, J.; Cui, Y. (2018). Design and self-assembly of hexahedral coordination cages for cascade reactions. Nat. Commun. *9*, 4423.

15. Takezawa, H.; Kanda, T.; Nanjo, H.; Fujita, M. (2019). Site-selective functionalization of linear diterpenoids through u-shaped folding in a confined artificial cavity. J. Am. Chem. Soc. *141*, 5112–5115.

16. Zhang, Q.; Tiefenbacher, K. (2013). Hexameric resorcinarene capsule is a Bronsted acid: investigation and application to synthesis and catalysis. J. Am. Chem. Soc *135*, 16213–16219.

17. For a recent review on the topic of substrate-selective catalysis see: Otte, M. (2016). Size-selective molecular flasks. ACS. Catal. *6*, 6491–6510.

18. Wang, Q. Q.; Gonell, S.; Leenders, S. H.; Durr, M.; Ivanovic-Burmazovic, I.; Reek, J. N. (2016). Self-assembled nanospheres with multiple endohedral binding sites pre-organize catalysts and substrates for highly efficient reactions. Nat. Chem. *8*, 225–230.

19. Osaki, M.; Takashima, Y.; Yamaguchi, H.; Harada, A. (2007). An artificial molecular chaperone: poly-pseudo-rotaxane with an extensible axle. J. Am. Chem. Soc. *129*, 14452–14457.

20. del Barrio, J.; Horton, P. N.; Lairez, D.; Lloyd, G. O.; Toprakcioglu, C.; Scherman, O. A. (2013). Photocontrol over cucurbit[8]uril complexes: stoichiometry and supramolecular polymers. J. Am. Chem. Soc. *135*, 11760–11763.

21. Thordarson, P.; Bijsterveld, E. J.; Rowan, A. E.; Nolte, R. J. (2003). Epoxidation of polybutadiene by a topologically linked catalyst. Nature *424*, 915–918.

22. Zheng, L.; Zhao, H.; Han, Y.; Qian, H.; Vukovic, L.; Mecinovic, J.; Kral, P.; Huck, W. T. S. (2019). Catalytic transport of molecular cargo using diffusive binding along a polymer track. Nat. Chem. *11*, 359–366.

23. Liu, Y.; Liu, X.; Warmuth, R. (2007). Multicomponent dynamic covalent assembly of a rhombicuboctahedral nanocapsule. Chem. Eur. J. *13*, 8953–8959.

24. Holst, J. R.; Trewin, A.; Cooper, A. I. (2010). Porous organic molecules. Nat. Chem. *2*, 915–920.

25. Mastalerz, M. (2010). Shape-persistent organic cage compounds by dynamic covalent bond formation. Angew. Chem. Int. Ed. *49*, 5042–5053.

26. Beuerle, F.; Gole, B. (2018). Covalent organic frameworks and cage compounds: design and applications of polymeric and discrete organic scaffolds. Angew. Chem. Int. Ed. *57*, 4850–4878.

27. Hasell, T.; Little, M. A.; Chong, S. Y.; Schmidtmann, M.; Briggs, M. E.; Santolini, V.; Jelfs, K. E.; Cooper, A. I. (2017). Chirality as a tool for function in porous organic cages. Nanoscale *9*, 6783–6790.

28. For reviews on the topic of imine-linked cages, see references 24, 25, 26, and 36.

29. Hasell, T.; Wu, X.; Jones, J. T.; Bacsa, J.; Steiner, A.; Mitra, T.; Trewin, A.; Adams, D. J.; Cooper, A. I. (2010). Triply interlocked covalent organic cages. Nat. Chem. *2*, 750–755.

30. Chen, L., et al. (2014). Separation of rare gases and chiral molecules by selective binding in porous organic cages. Nat. Mater. *13*, 954–960.

31. Ding, H.; Wu, X.; Zeller, M.; Xie, Y.; Wang, C. (2015). Controllable synthesis of covalent porphyrinic cages with varying sizes via template-directed imine condensation reactions. J. Org. Chem. *80*, 9360–9364.

32. Kandambeth, S.; Venkatesh, V.; Shinde, D. B.; Kumari, S.; Halder, A.; Verma, S.; Banerjee, R. (2015). Self-templated chemically stable hollow spherical covalent organic framework. Nat. Commun. *6*, 6786.

33. Ronson, T. K.; Meng, W.; Nitschke, J. R. (2017). Design principles for the optimization of guest binding in aromatic-paneled $Fe(II)_4L_6$ cages. J. Am. Chem. Soc. *139*, 9698–9707.

34. Cao, N.; Wang, Y.; Zheng, X.; Jiao, T.; Li, H. (2018). Controllable self-assembly of pills and cages via imine condensation for silver cation detection. Org. Lett. *20*, 7447–7450.

35. Greenaway, R. L., et al. (2018). High-throughput discovery of organic cages and catenanes using computational screening fused with robotic synthesis. Nat. Commun. *9*, 2849.

36. Mastalerz, M. (2018). Porous shape-persistent organic cage compounds of different size, geometry, and function. Acc. Chem. Res *51*, 2411–2422.

37. Zhang, X.; Li, H.; Zhang, L.; Kong, F.; Fan, D.; Wang, W. (2018). Porous Organic cage embedded C18 amide silica stationary phase for high performance liquid chromatography. Anal. Sci. *34*, 445–451.

38. Hussain, M. D. W.; Giri, A.; Patra, A. (2019). Organic nanocages: a promising testbed for catalytic CO_2 conversion. Sustainable Energy Fuels, *3*, 2567–2571.

39. Ciaccia, M.; Cacciapaglia, R.; Mencarelli, P.; Mandolini, L.; Di Stefano, S. (2013). Fast transimination in organic solvents in the absence of proton and metal catalysts. A key to imine metathesis catalyzed by primary amines under mild conditions. Chem. Sci. *4*, 2253–2261.

40. Laha, J. K.; Tummalapalli, K. S.; Jethava, K. P. (2016). Implications of dynamic imine chemistry for the sustainable synthesis of nitrogen heterocycles via transimination followed by intramolecular cyclisation. Org. Biomol. Chem. *14*, 2473–2479.

41. One possible drawback of imine cages is that the imine bonds of the catalyst would engage in transimination side reactions (see references 39 and 40 for examples) with the amines of the polymers.

42. Mosquera, J.; Zarra, S.; Nitschke, J. R. (2014). Aqueous anion receptors through reduction of subcomponent self-assembled structures. Angew. Chem. Int. Ed. *53*, 1556–1559.

43. Skene, W. G.; Lehn, J. M. (2004). Dynamers: polyacylhydrazone reversible covalent polymers, component exchange, and constitutional diversity. Proc. Natl. Acad. Sci. U.S.A. *101*, 8270–8275.

44. Ferguson, J. S.; Yamato, K.; Liu, R.; He, L.; Zeng, X. C.; Gong, B. (2009). One-pot formation of large macrocycles with modifiable peripheries and internal cavities. Angew. Chem. Int. Ed. *48*, 3150–3154.

45. Bhat, V. T.; Caniard, A. M.; Luksch, T.; Brenk, R.; Campopiano, D. J.; Greaney, M. F. (2010). Nucleophilic catalysis of acylhydrazone equilibration for protein-directed dynamic covalent chemistry. Nat. Chem. *2*, 490–497.

46. Klein, J. M.; Saggiomo, V.; Reck, L.; Luning, U.; Sanders, J. K. (2012). Dynamic combinatorial libraries for the recognition of heavy metal ions. Org. Biomol. Chem. *10*, 60–66.

47. Lin, Z.; Emge, T. J.; Warmuth, R. (2011). Multicomponent assembly of cavitand-based polyacylhydrazone nanocapsules. Chem. Eur. J. *17*, 9395–9405.

48. Harder, E., et al. (2016). OPLS3: A force field providing broad coverage of drug-like small molecules and proteins. J. Chem. Theory. Comput. *12*, 281–296.

49. Li, H.; Zhang, H.; Lammer, A. D.; Wang, M.; Li, X.; Lynch, V. M.; Sessler, J. L. (2015). Quantitative self-assembly of a purely organic three-dimensional catenane in water. Nat. Chem. *7*, 1003–1008.

50. Shen, L., et al. (2018). Dynamic covalent self-assembly based on oxime condensation. Angew. Chem. Int. Ed. *57*, 16486–16490.

51. Sharafi, M.; Campbell, J. P.; Rajappan, S. C.; Dudkina, N.; Gray, D. L.; Woods, T. J.; Li, J.; Schneebeli, S. T. (2017). Crystal packing-driven enrichment of atropoisomers. Angew. Chem. Int. Ed. *56*, 7097−7101.

52. Dalcanale, E.; Montanari, F. (1986). Selective oxidation of aldehydes to carboxylic acids with sodium chlorite-hydrogen peroxide. J. Org. Chem. *51*, 567–569.

53. Li, W.; Chung, H.; Daeffler, C.; Johnson, J. A.; Grubbs, R. H. (2012). Application of ^{1}H DOSY for facile measurement of polymer molecular weights. Macromol. *45*, 9595–9603.

54. The percentage of polymer chains complexed to **Tet-1** is highest at the titration point with [**Short-NH_2-POA**] = 0.26 mM and [**Tet-1**] = 0.28 mM. A smaller percentage of the polymers are complexed to the **Tet-1** receptor at the titration point with [**Short-NH_2-POA**] = 0.50 mM. Thus, based on the data shown in Figure 5a, the resonances of **NH_2-POA** clearly shift downfield upon complexation to **Tet-1**.

55. Wannere, C. S.; Schleyer, P. V. (2003). How do ring currents affect ^{1}H NMR chemical shifts? Org. Lett. *5*, 605–608.

56. Liu, Z.; Nalluri, S. K. M.; Stoddart, J. F. (2017). Surveying macrocyclic chemistry: from flexible crown ethers to rigid cyclophanes. Chem. Soc. Rev. *46*, 2459–2478.

57. Stoddart, J. F. (2017). Mechanically interlocked molecules (MIMs)-molecular shuttles, switches, and machines (Nobel lecture). Angew. Chem. Int. Ed. *56*, 11094–11125.

58. Kovrigin, E. L. (2012). NMR line shapes and multi-state binding equilibria. J. Biomol. NMR *53*, 257-270.

59. Virtanen, P., et al. (2019). SciPy 1.0 — Fundamental algorithms for scientific computing in python. arXiv, 1907.10121.

60. Wang, X.; Wicher, B.; Ferrand, Y.; Huc, I. (2017). Orchestrating directional molecular motions: kinetically controlled supramolecular pathways of a helical host on rodlike guests. J. Am. Chem. Soc. *139*, 9350–9358.

61. Albery, W. J.; Knowles, J. R. (1976). Evolution of enzyme function and the development of catalytic efficiency. Biochemistry *15*, 5631–5640.

62. Basilio, N.; Garcia-Rio, L.; Mejuto, J. C.; Perez-Lorenzo, M. (2006). A new reaction pathway in the ester aminolysis catalyzed by glymes and crown ethers. J. Org. Chem. *71*, 4280–4285.

63. Maude, A. B.; Williams, A. (1995). Complexation catalysis: effective charge development in the aminolysis of phenyl esters in chlorobenzene catalysed by crown ethers. J. Chem. Soc., Perkin Trans. 2, 691–696.

64. Basilio, N.; García-Río, L.; Peña-Gallego, Á.; Pérez-Lorenzo, M. (2012). Molecular recognition-based catalysis in nucleophilic aromatic substitution: a mechanistic study. New J. Chem. *36*, 1519–1526.

65. Yamashina, M.; Kusaba, S.; Akita, M.; Kikuchi, T.; Yoshizawa, M. (2018). Cramming versus threading of long amphiphilic oligomers into a polyaromatic capsule. Nat. Commun. *9*, 4227.

66. Riess, B.; Wanzke, C.; Tena-Solsona, M.; Grotsch, R. K.; Maity, C.; Boekhoven, J. (2018). Dissipative assemblies that inhibit their deactivation. Soft Matter *14*, 4852–4859.

67. Qian, H.; Wang, Y. Y.; Guo, D. S.; Aprahamian, I. (2017). Controlling the isomerization rate of an Azo-BF_2 switch using aggregation. J. Am. Chem. Soc. *139*, 1037–1040.

68. Roos, K., et al. (2019). OPLS3e: Extending force field coverage for drug-like small molecules. J. Chem. Theory. Comput. *15*, 1863–1874.

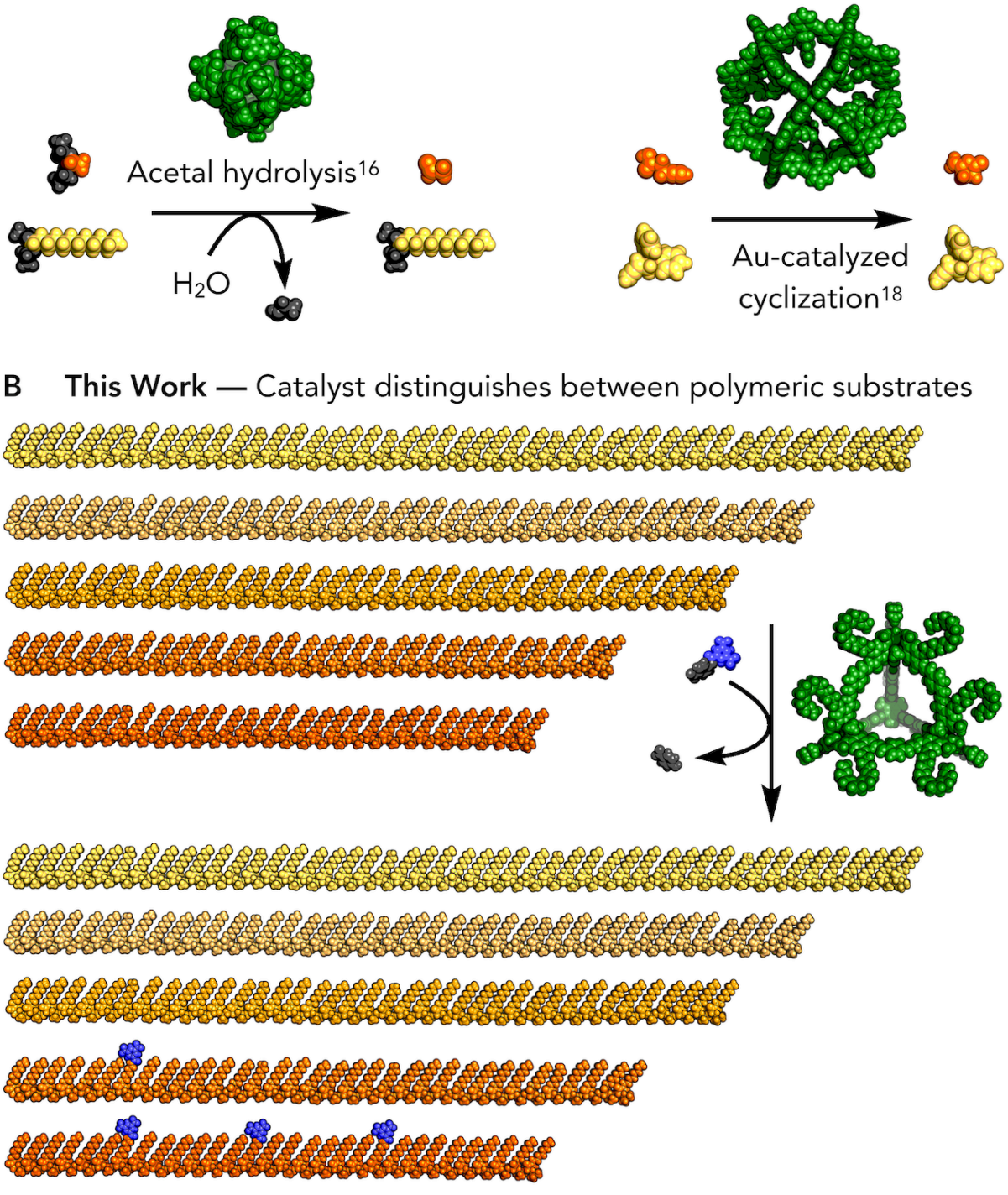
A Examples from prior work (see ref. 17 for a review) — Catalyst distinguishes between two small-molecule substrates
Acetal hydrolysis[16]
H_2O
Au-catalyzed cyclization[18]
B This Work — Catalyst distinguishes between polymeric substrates

Figure 1

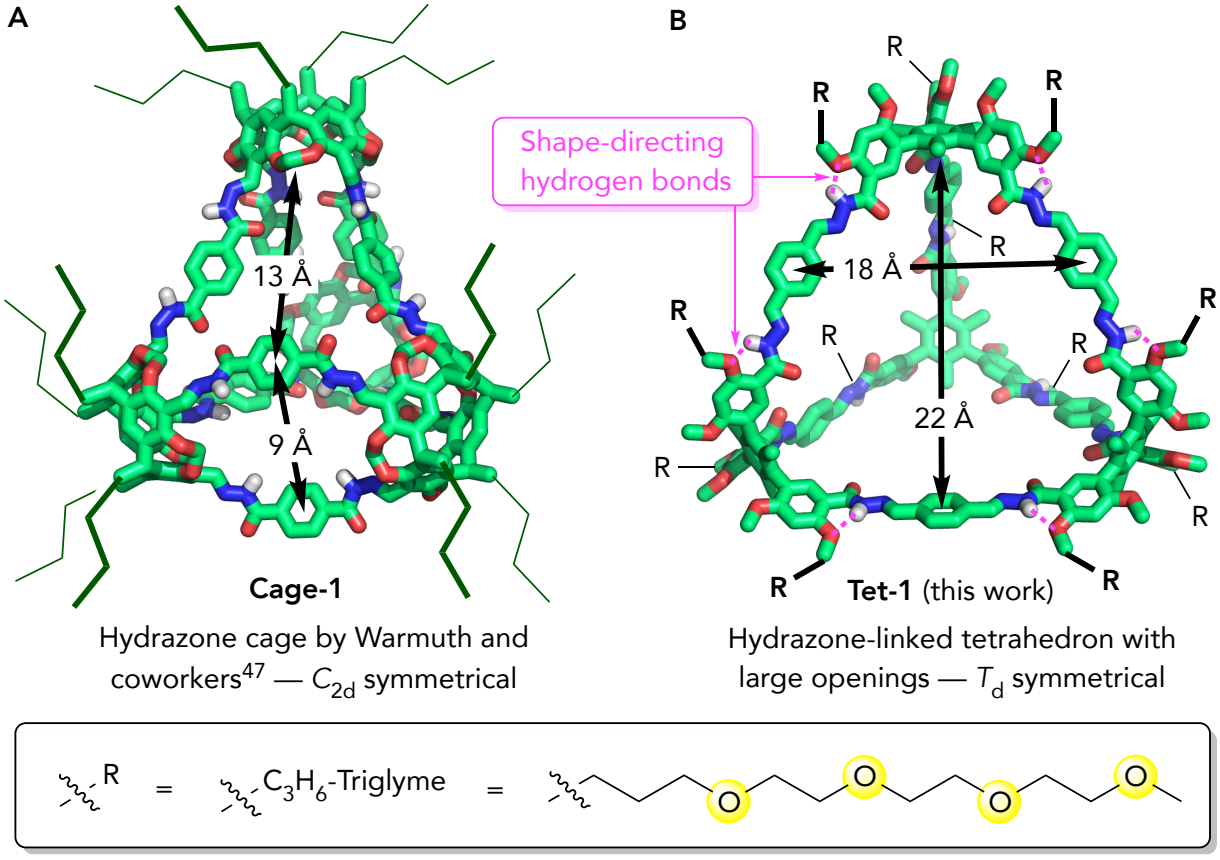
A
13 Å
9 Å
Cage-1
Hydrazone cage by Warmuth and coworkers[47] — C_{2d} symmetrical
B
Shape-directing hydrogen bonds
R
18 Å
22 Å
Tet-1 (this work)
Hydrazone-linked tetrahedron with large openings — T_d symmetrical
R = C_3H_6-Triglyme =
O

Figure 2

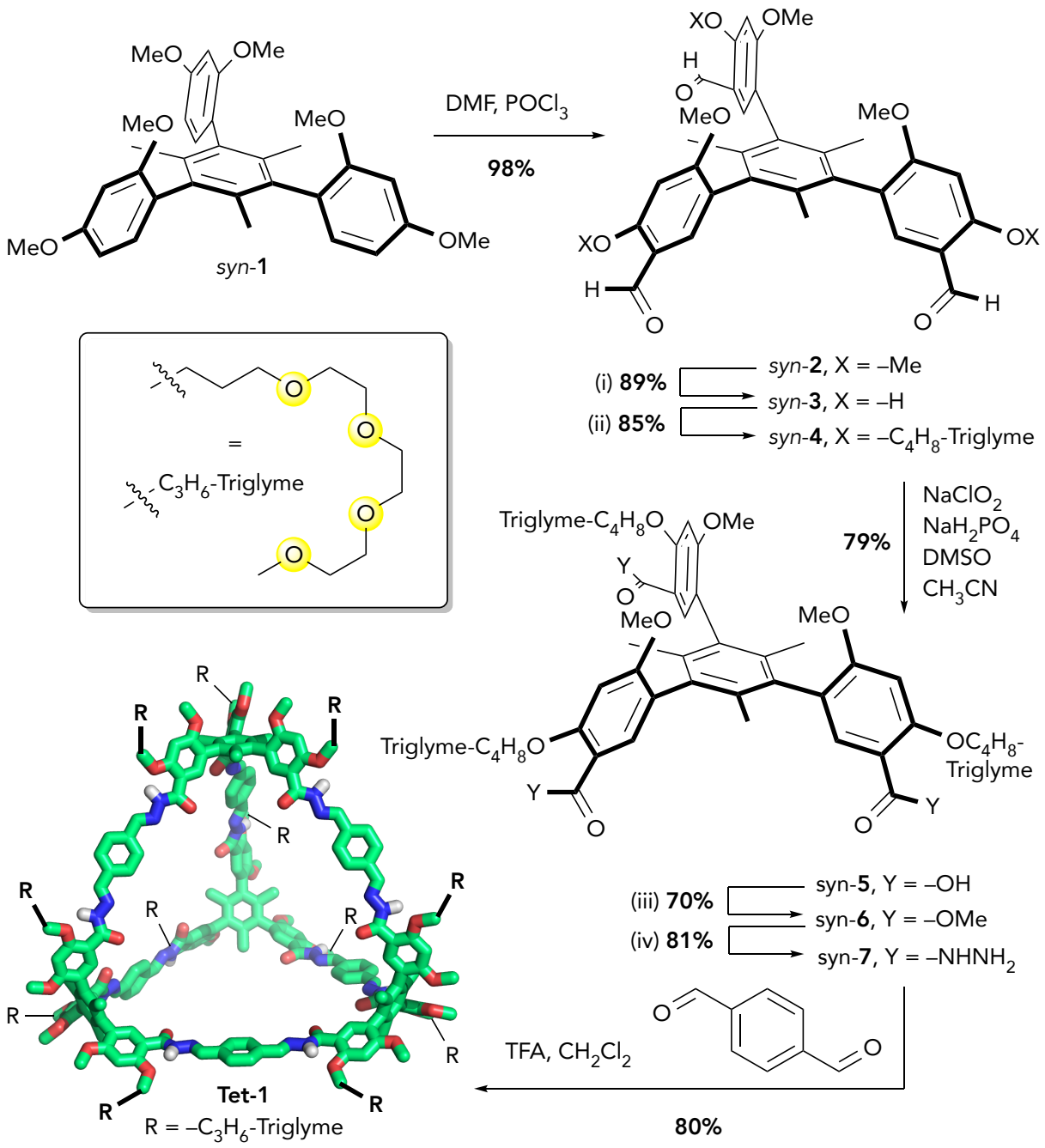
MeO
OMe
MeO
MeO
MeO
OMe
syn-1
DMF, POCl3
98%
XO
OMe
H
O
MeO
MeO
XO
OX
H
O
H
O
(i) 89%
syn-2, X = –Me
(ii) 85%
syn-3, X = –H
syn-4, X = –C4H8-Triglyme
=
C3H6-Triglyme
O
O
O
O
Triglyme-C4H8O
OMe
Y
O
MeO
MeO
79%
NaClO2
NaH2PO4
DMSO
CH3CN
Triglyme-C4H8O
OC4H8-
Triglyme
Y
O
Y
O
R
R
R
R
R
R
R
R
R
R
R
R
Tet-1
R = –C3H6-Triglyme
(iii) 70%
syn-5, Y = –OH
(iv) 81%
syn-6, Y = –OMe
syn-7, Y = –NHNH2
O
O
TFA, CH2Cl2
80%

Scheme 1

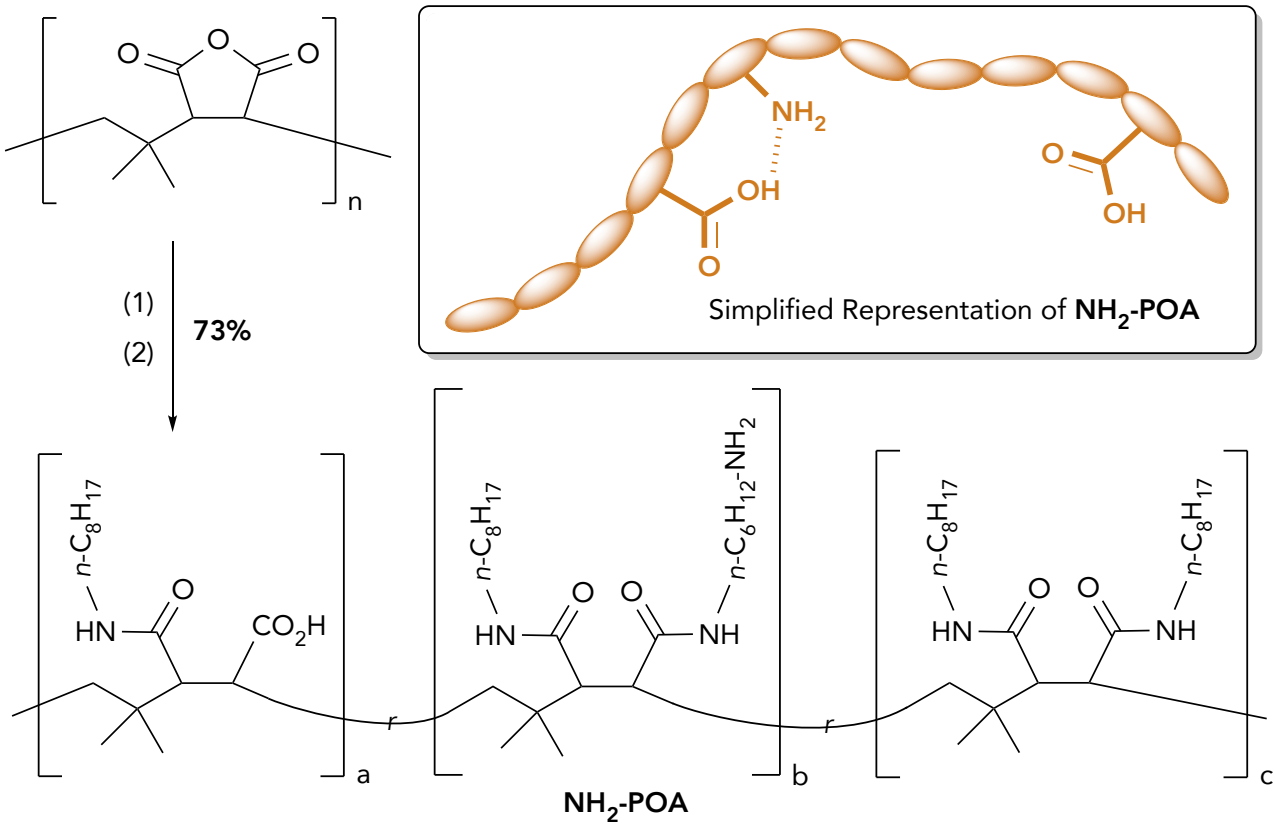

Scheme 2

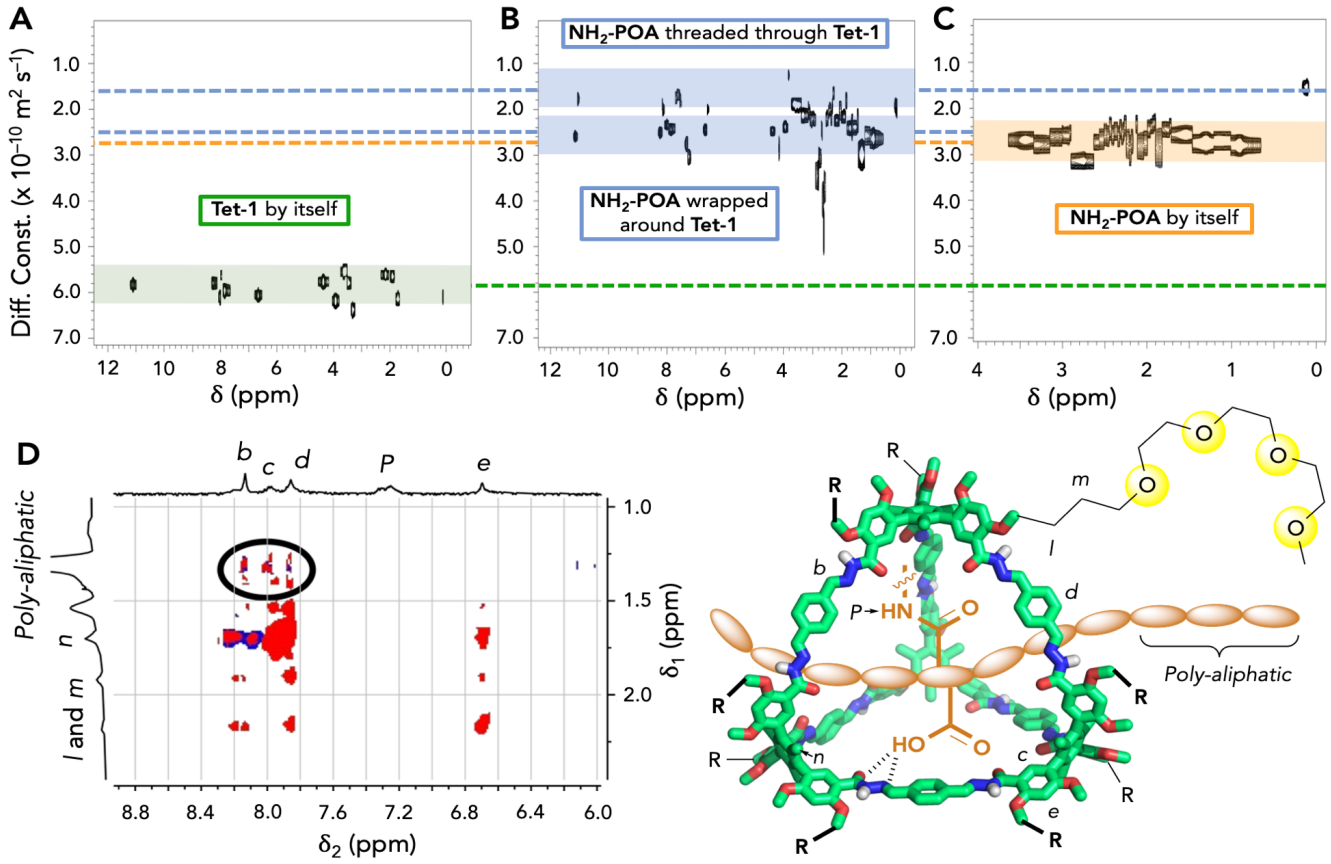
A
B
C
Diff. Const. (x 10⁻¹⁰ m² s⁻¹)
Tet-1 by itself
NH2-POA threaded through Tet-1
NH2-POA wrapped around Tet-1
NH2-POA by itself
δ (ppm)
D
b
c
d
P
e
Poly-aliphatic
n
l and m
δ1 (ppm)
δ2 (ppm)
R
m
l
b
d
P→HN
HO
c
n
e
Poly-aliphatic

Figure 3

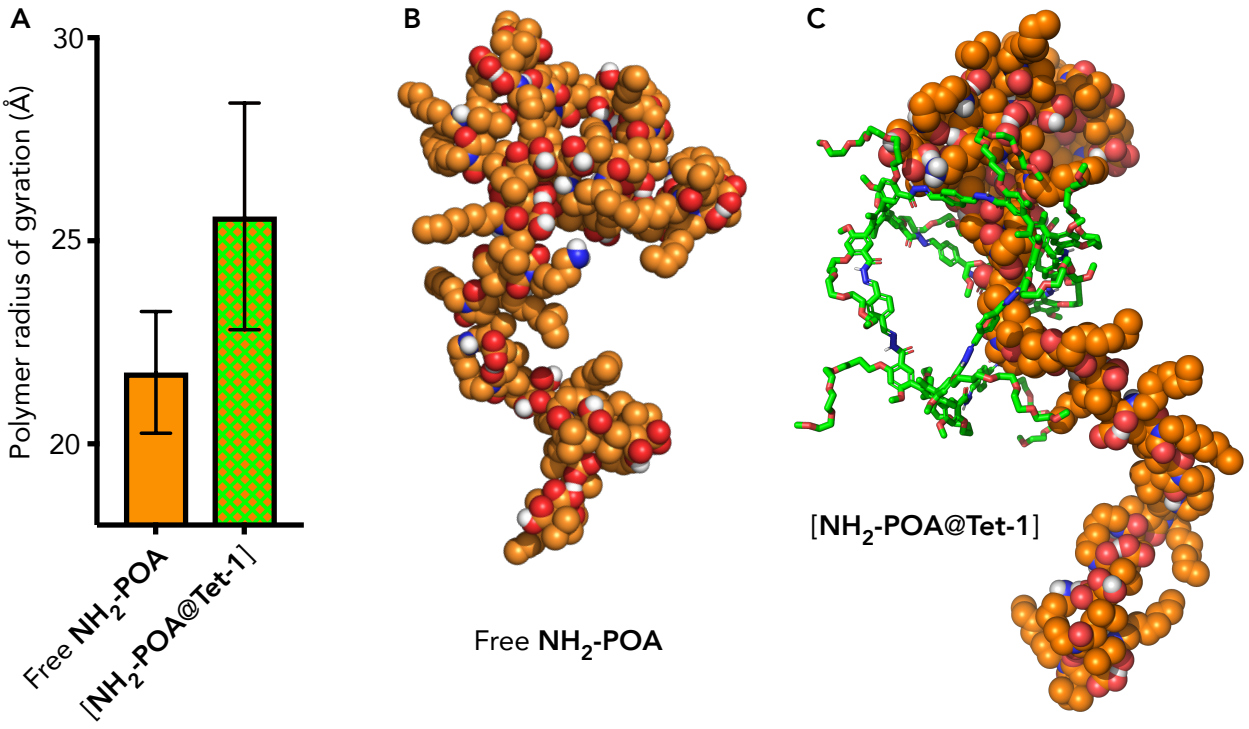
A
30
25
20
Polymer radius of gyration (Å)
Free NH2-POA
[NH2-POA@Tet-1]
B
Free NH2-POA
C
[NH2-POA@Tet-1]

Figure 4

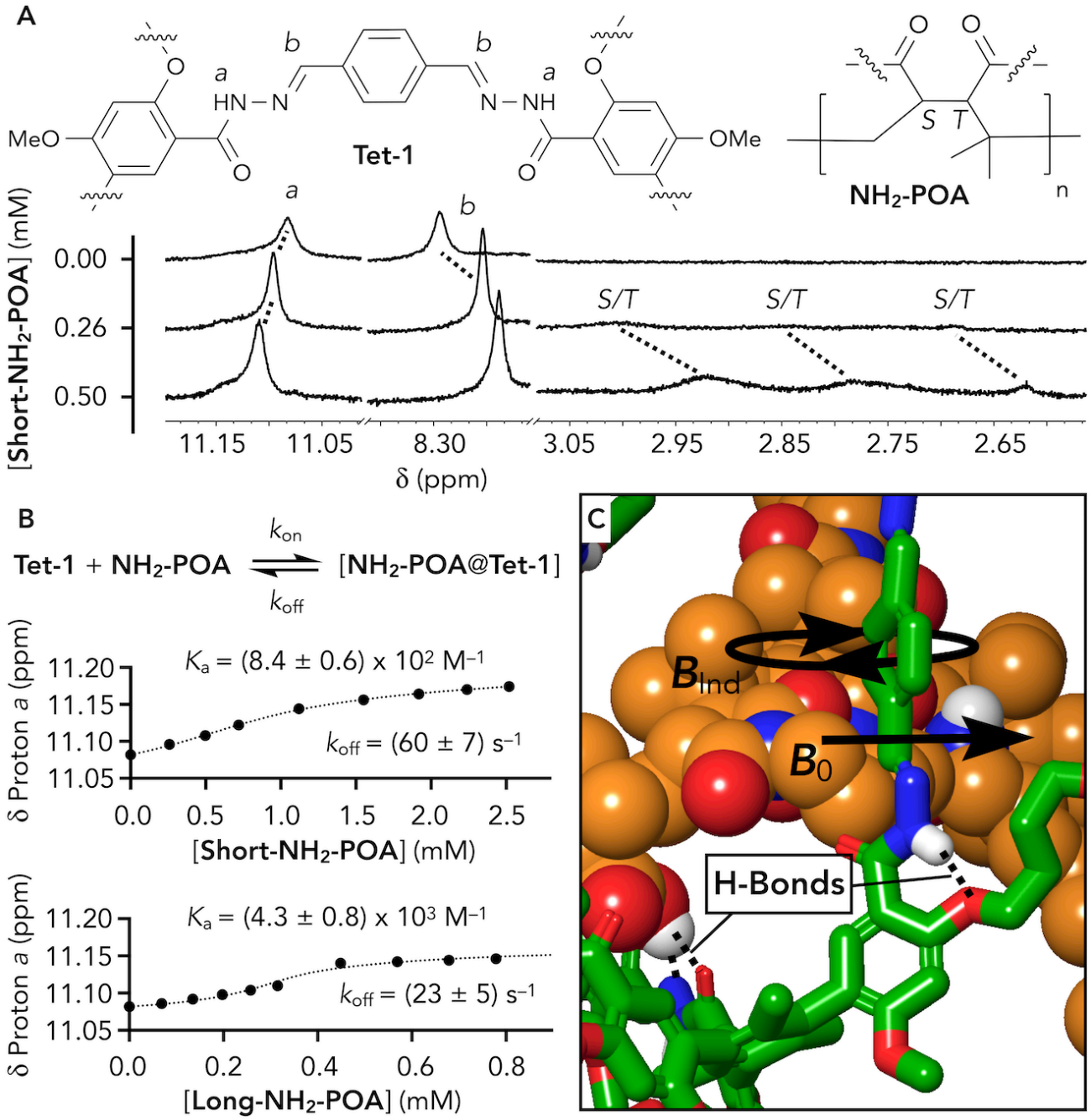
A
MeO
OMe
Tet-1
NH2-POA
S T
n
a
b
[Short-NH2-POA] (mM)
0.00
0.26
0.50
S/T
S/T
S/T
11.15
11.05
8.30
3.05
2.95
2.85
2.75
2.65
δ (ppm)
B
Tet-1 + NH2-POA
kon
koff
[NH2-POA@Tet-1]
δ Proton a (ppm)
Ka = (8.4 ± 0.6) x 10² M⁻¹
koff = (60 ± 7) s⁻¹
[Short-NH2-POA] (mM)
Ka = (4.3 ± 0.8) x 10³ M⁻¹
koff = (23 ± 5) s⁻¹
[Long-NH2-POA] (mM)
C
BInd
B0
H-Bonds

Figure 5

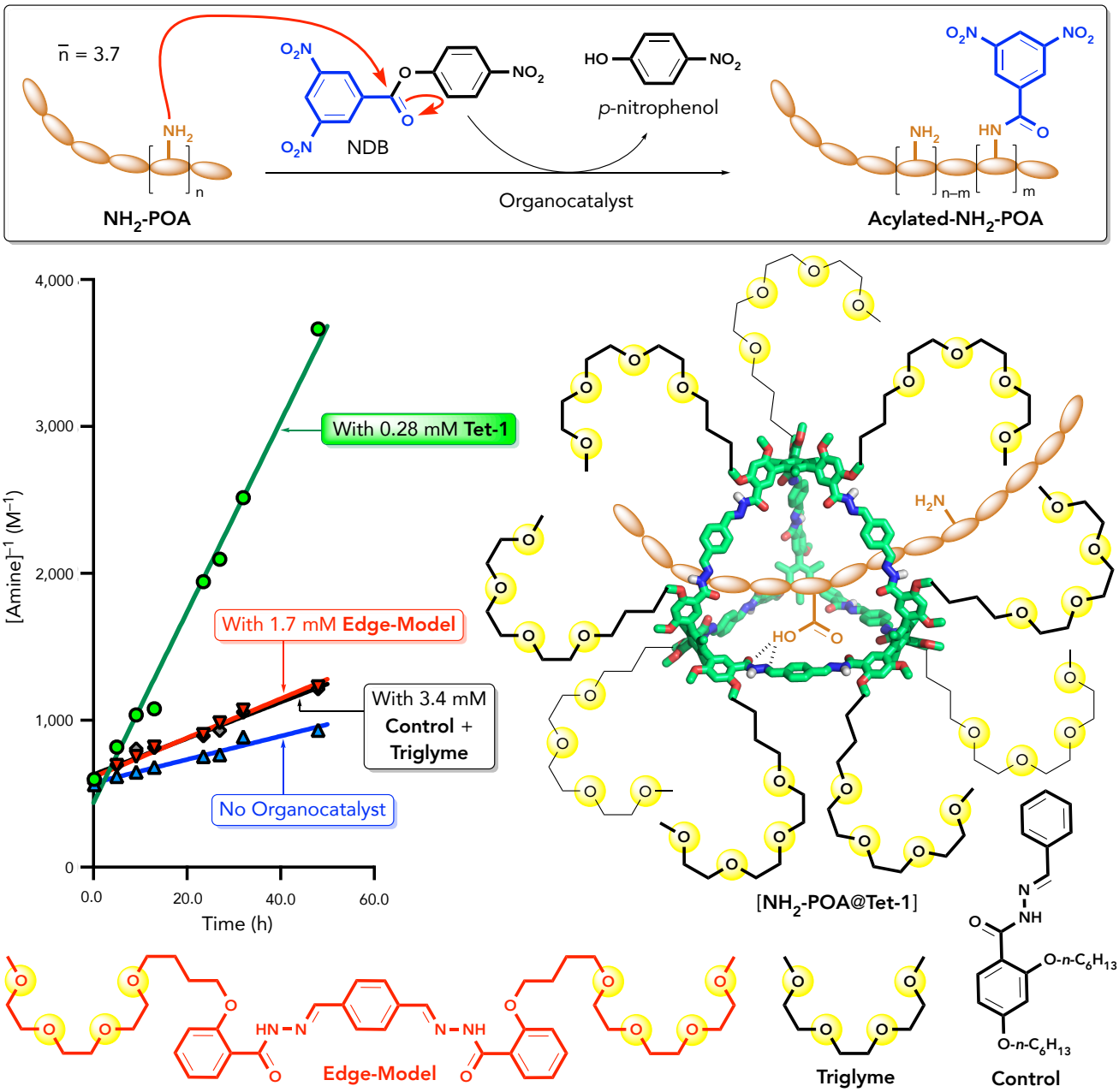
n̄ = 3.7
NH2
n
NH2-POA
O2N
NO2
O
NDB
HO
NO2
p-nitrophenol
Organocatalyst
HN
n–m
m
Acylated-NH2-POA
4,000
3,000
2,000
1,000
0
[Amine]−1 (M−1)
0.0
20.0
40.0
60.0
Time (h)
With 0.28 mM Tet-1
With 1.7 mM Edge-Model
With 3.4 mM Control + Triglyme
No Organocatalyst
H2N
HO
[NH2-POA@Tet-1]
HN
N
Edge-Model
Triglyme
NH
O-n-C6H13
Control

Figure 6

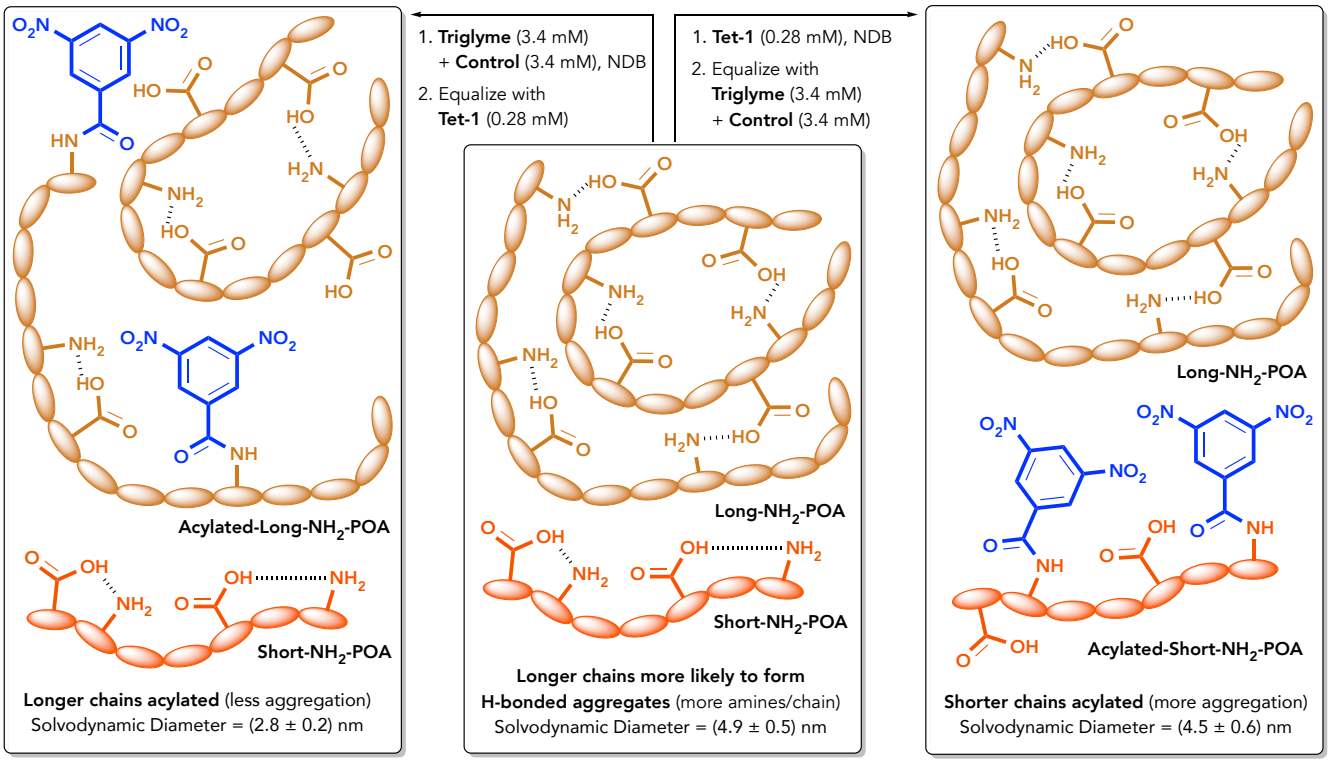
1. Triglyme (3.4 mM)
+ Control (3.4 mM), NDB
2. Equalize with
Tet-1 (0.28 mM)
1. Tet-1 (0.28 mM), NDB
2. Equalize with
Triglyme (3.4 mM)
+ Control (3.4 mM)
Acylated-Long-NH2-POA
Short-NH2-POA
Longer chains acylated (less aggregation)
Solvodynamic Diameter = (2.8 ± 0.2) nm
Long-NH2-POA
Short-NH2-POA
Longer chains more likely to form
H-bonded aggregates (more amines/chain)
Solvodynamic Diameter = (4.9 ± 0.5) nm
Long-NH2-POA
Acylated-Short-NH2-POA
Shorter chains acylated (more aggregation)
Solvodynamic Diameter = (4.5 ± 0.6) nm

Figure 7

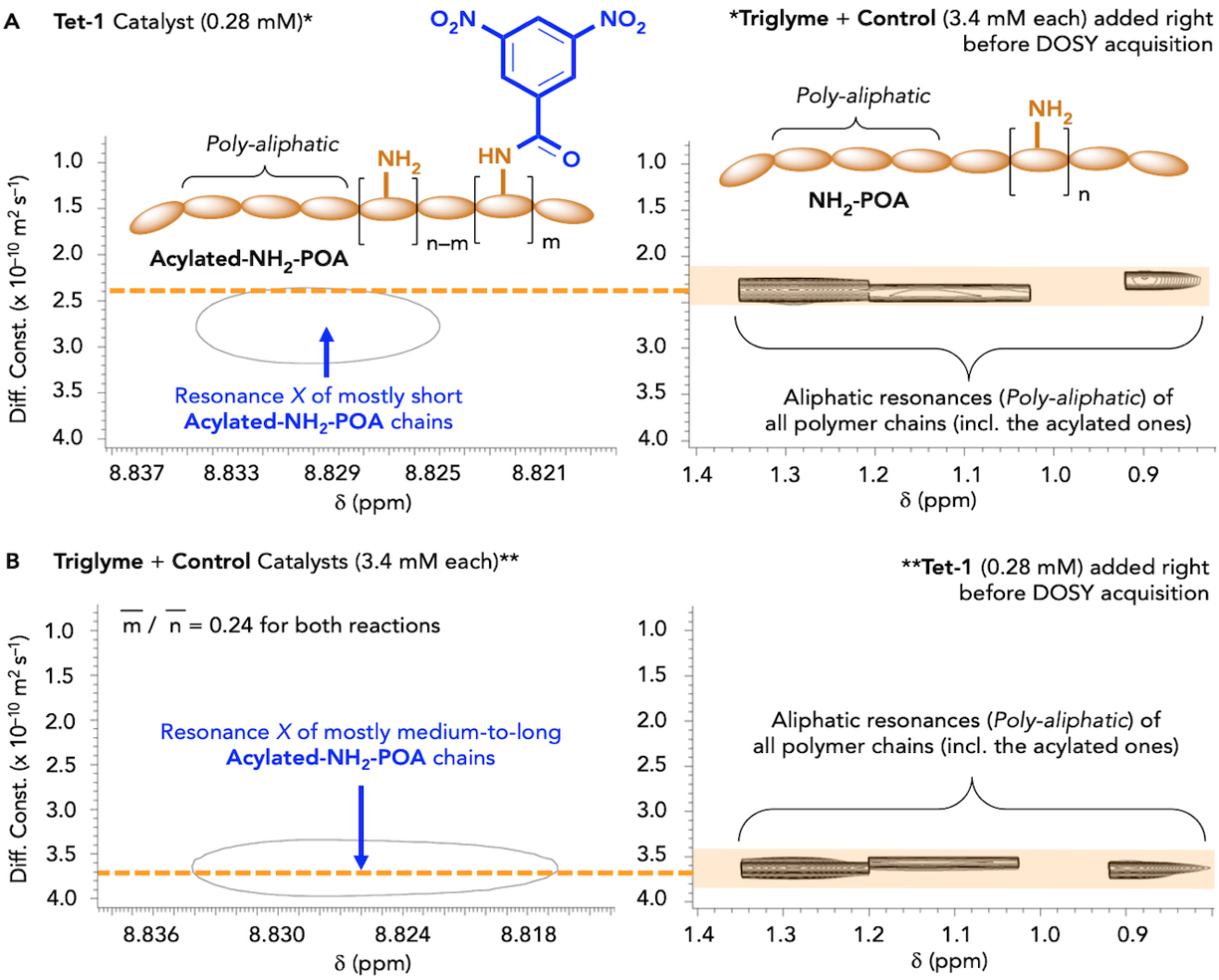
A
Tet-1 Catalyst (0.28 mM)*
*Triglyme + Control (3.4 mM each) added right before DOSY acquisition
Poly-aliphatic
NH2
HN
O
O2N
NO2
n–m
m
Acylated-NH2-POA
Resonance X of mostly short Acylated-NH2-POA chains
Diff. Const. (x 10−10 m2 s−1)
δ (ppm)
Poly-aliphatic
NH2
NH2-POA
n
Aliphatic resonances (Poly-aliphatic) of all polymer chains (incl. the acylated ones)
B
Triglyme + Control Catalysts (3.4 mM each)**
**Tet-1 (0.28 mM) added right before DOSY acquisition
m / n = 0.24 for both reactions
Resonance X of mostly medium-to-long Acylated-NH2-POA chains
Aliphatic resonances (Poly-aliphatic) of all polymer chains (incl. the acylated ones)

Figure 8

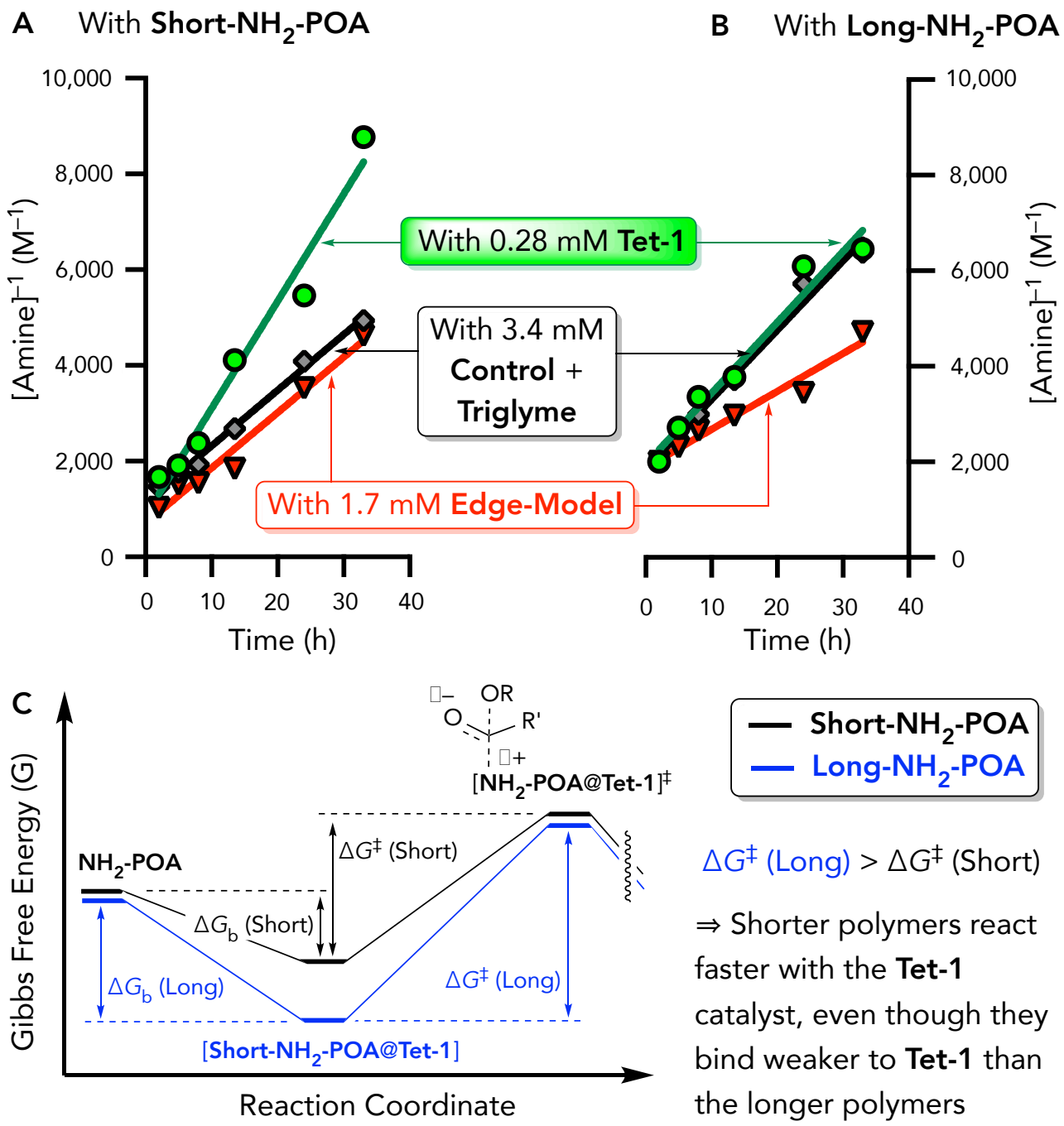
A With Short-NH2-POA
B With Long-NH2-POA
10,000
8,000
6,000
4,000
2,000
0
[Amine]−1 (M−1)
0 10 20 30 40
Time (h)
With 0.28 mM Tet-1
With 3.4 mM Control + Triglyme
With 1.7 mM Edge-Model
C
Gibbs Free Energy (G)
NH2-POA
ΔG‡ (Short)
ΔGb (Short)
ΔGb (Long)
ΔG‡ (Long)
[Short-NH2-POA@Tet-1]
[NH2-POA@Tet-1]‡
Reaction Coordinate
Short-NH2-POA
Long-NH2-POA
ΔG‡ (Long) > ΔG‡ (Short)
⇒ Shorter polymers react faster with the Tet-1 catalyst, even though they bind weaker to Tet-1 than the longer polymers

Figure 9

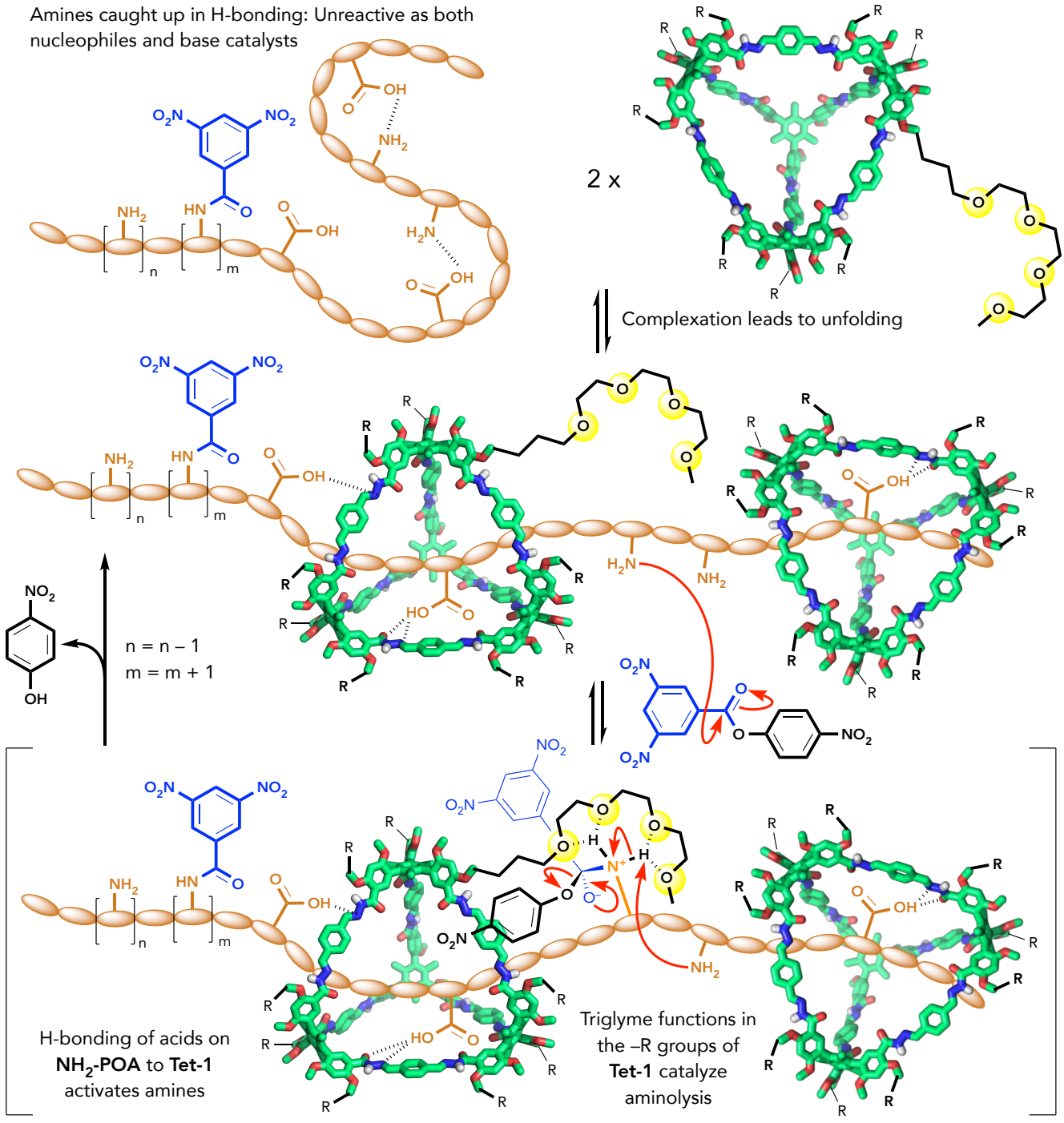
Amines caught up in H-bonding: Unreactive as both nucleophiles and base catalysts
2 x
Complexation leads to unfolding
n = n – 1
m = m + 1
H-bonding of acids on NH2-POA to Tet-1 activates amines
Triglyme functions in the –R groups of Tet-1 catalyze aminolysis

Scheme 3

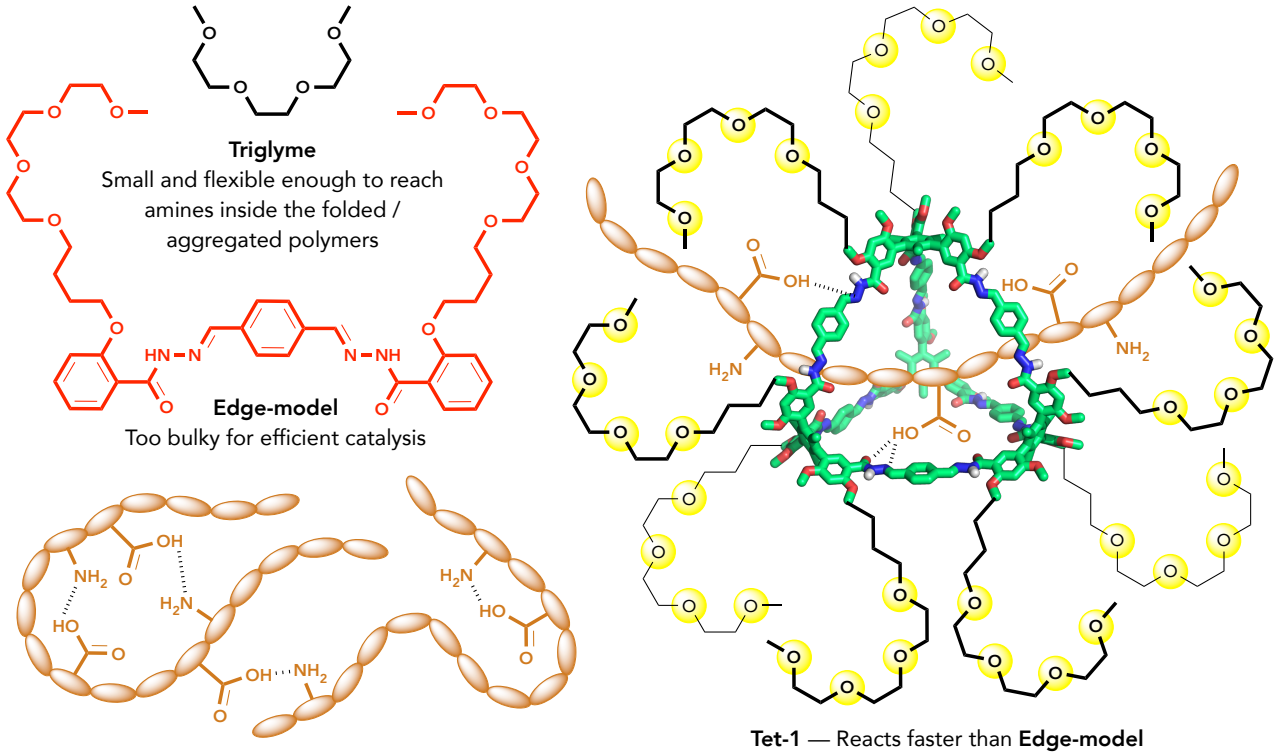

Long-NH$_2$-POA in the abscence of **Tet-1**

Tet-1 — Reacts faster than **Edge-model** with **Long-NH$_2$-POA** since it can unfold / break apart the polymers

Figure 10

The Bigger Picture

Nature employs sophisticated catalysts to selectively functionalize biopolymers after they have already been synthesized. Yet, despite plenty of examples in biology, efficient and selective modification of man-made polymers is still difficult. Many functional polymers with complex topologies cannot be generated in high yields with traditional methods. Thus, catalysts able to derivatize man-made polymers for desirable polymeric size, sequence, and folded topology are in critical need, for future advances in fields such as medicine, electronics, and renewable energy. This work now provides one of the first examples for selective catalysis with polymeric substrates. We show that stable synthetic catalysts with large openings can distinguish between polymer chains of various lengths in a complex mixture, providing proof-of-principle for selective catalytic polymer functionalization. This concept will be applied to prepare otherwise inaccessible polymers in the future.

Highlights

We synthesized a catalytically-active, hydrazone-linked molecular tetrahedron

The tetrahedron threads over polymeric substrates to disentangle them

Short polymers are functionalized selectively with the catalytic tetrahedron

Our results suggest untapped potential for selective polymer functionalization

eTOC Blurb

We report an original catalytic molecular tetrahedron. By threading through the cavity of the tetrahedron, polymeric substrates are unfolded or broken apart. Our catalyst distinguishes between polymer chains of different lengths, functionalizing the shorter polymers selectively over the longer ones — as a proof-of-concept for selective catalysis to modify polymers. Our findings advance the fundamental understanding of the thermodynamic and kinetic phenomena controlling the interactions between molecular cages and synthetic polymers, offering valuable ability to create complex materials in the future.